2018

Facilitated Excretion of Gold Nanoparticles by Copper Sulfide Nanoparticles Through the ATP7B Transporter

Xiaodong Wang
University of Rhode Island, xiaodong.wang0609@gmail.com

FACILITATED EXCRETION OF GOLD NANOPARTICLES BY COPPER SULFIDE NANOPARTICLES THROUGH THE ATP7B TRANSPORTER

BY

XIAODONG WANG

A DISSERTATION SUBMITTED IN PARTIAL FULFILLMENT OF THE REQUIREMENTS FOR THE DEGREE OF

DOCTOR OF PHILOSOPHY

IN

BIOMEDICAL AND PHARMACEUTICAL SCIENCE

UNIVERSITY OF RHODE ISLAND

2018

DOCTOR OF PHILOSOPHY DISSERTATION

OF

XIAODONG WANG

APPROVED:

Dissertation Committee:

Major Professor Bingfang Yan

Yuan Zhang

Hongyuan Yuan

Nasser H. Zawia

DEAN OF THE GRADUATE SCHOOL

UNIVERSITY OF RHODE ISLAND

2018

ABSTRACT

Scientific areas have utilized the exclusive qualities of nanomaterials for medicine, diagnostics, drug delivery, tissue engineering and environmental protection. Inorganic metal nanoparticles such as gold and copper have been widely studied in the past decades. Due to the strong and tunable surface plasmon resonance (SPR), nanostructures including nanoshells, nanorods, nanocages, and hollow nanospheres exhibit strong optical absorption at near-infrared (NIR) wavelengths (650–900 nm), resulting in resonance and transfer of thermal energies to the surrounding tissue to raise the temperature. The absorbance of NIR light is desirable because it minimizes thermal injury to normal tissues while providing optimal light penetration. The efficient photothermal energy transfer effect by inorganic metallic nanoparticles such as gold has been widely used for photothermal ablation of tumor tissues, as well as drug delivery system for small molecules like protein, antibodies, DNAs, and small interfering RNAs by NIR laser triggered-release.

Even though different kinds of gold nanoparticles have a great advantage on the photothermal transaction and are promising for clinical applications, they are non-biodegradable, raising concerns regarding their short/long-term metabolism and safety. Tail vein injections of polyethylene glycol (PEG)-coated gold nanoparticles have been reported to induce two phases of toxicity concerning inflammation in the liver. The acute phase occurred immediately after administration of nanoparticles. The second phase happened at 7 days post injection when the nanoparticles become localized in the tissues, mostly in the liver and spleen after circulation in the blood. Due to multiple valences of gold, redox reaction of gold within cells can increase the levels of

reactive oxygen species (ROS), which interferes with the mitochondrial membrane potential. Disturbance of the mitochondrial membrane potential after exposure to gold nanoparticles initiates an apoptotic cascade in cells.

It was also reported that three months after injection of PEG-HAuNPs, 11.4 ± 1.8 percentage of injected dose per gram (%ID/g) remained in liver, which was 70% of the amount at one-day post injection. However, three months after injection of PEG-HCuSNPs, the Cu level remaining in the liver was 1.1 ± 0.1 %ID/g, which was only 5% of the amount at 1 day post injection. The Cu level in the liver decreases much faster than Au level after 1 day, indicating faster metabolism and excretion of copper nanoparticles than the gold nanoparticles.

Based on the previous research and findings, although gold nanoparticles have more efficient photothermal transfer and more potential of future clinical usage for tumor tissue ablation, they have a very slow metabolic and excretion rate, which leads to acute and chronic *in vivo* toxicity. These findings support the hypothesis that conjugating copper with gold nanoparticles will increase the *in vivo* excretion rate of gold to reduce its toxicity while retaining the more efficient photothermal transfer properties of gold nanoparticles for future clinical application.

Manuscript 1: Introduction to Metal Nanoparticles: Application in Pharmaceutical Sciences *(to be submitted to Materials Chemistry and Physics)* reviews the development and promising application of metal nanoparticles in pharmaceutical and biomedical industry including, but not limited to, drug delivery, *in vivo* imaging, *in vitro* diagnostics, therapeutics techniques, toxicity, etc.

Manuscript 2: Enhanced Cellular Clearance of Gold Nanoparticles by Copper Sulfide Nanoparticles Through ATP7B as Transporter. *(to be submitted to ACS Nano)* In this study, we use PEGylated hollow CuS nanoparticles (PEG-HCuSNPs) of ~70 nm in diameter as models to elucidate their highly efficient metabolic trafficking in mouse liver. The Cu-ATPase transporter, ATP7B efficiently facilitates removal of excess Cu ions in hepatocytes. ATP7B together with PEG-HCuSNPs-loaded lysosomes move toward the apical domains of hepatocytes to transfer Cu into the bile canaliculi through exocytosis. Moreover, primary cultured mouse hepatocytes exhibit much higher efficient copper exocytosis than primary cultured mouse Kupffer cells. Tail vein injections of polyethylene glycol (PEG)-coated gold nanoparticles have been reported to induce two phases of toxicity concerning inflammation in mouse liver. Conjugating copper with gold nanoparticles will increase the *in vivo* excretion rate of gold to reduce its toxicity by fast metabolism and excretion rate of copper while retaining the more efficient photothermal transfer properties of gold nanoparticles for the future clinical application.

ACKNOWLEDGEMENTS

First, I would like to express my sincere gratitude to my advisor Prof. Bingfang Yan, for his continuous support of my Ph.D. study and related research for the past years. He is always open to any questions and provides valuable suggestions not only in my academic study to be a better scientist, but also in daily life to be a better person. Also, I would like to express my deepest gratitude to my mentor Dr. Wei Lu during my Ph.D. study. His guidance helped me all the time during my research. I could not make this achievement without his patience, enthusiasm, and expertise in the research. I could not have imagined having a better advisor and mentor guiding me in my study. Mine sincerely thanks to Dr. Hongyan Yuan, Dr. Yuan Zhang, Dr. Maggie Charpentier and Dr. Xinyuan Chen for being my committee members and giving me advice on my comprehensive exam and project.

I would like to thank my colleagues in Dr. Yan lab for their help during my study. A special thanks go to Dr. Yi-Tzai Chen for his guidance in the animal study and also Dr. Liangran Guo, for advising me on nanoparticle synthesis. Thanks to Dr. Al Bach and Kim Andrews in INBRE for helping me with the instruments, and also, Gerralyn Perry and Kathleen Hayes for their help during my study. My research would not have been possible without their support.

I would like to thank my parents, my parents-in-law and other family members for their support. Last but the most important, I'd like to thank my dear wife Yi and

my lovely daughter Elaine for their courage and standing by me in good and bad times throughout my Ph.D. study.

PREFACE

This dissertation was prepared according to the University of Rhode Island "Guidelines for the Format of Theses and Dissertations" standards for the Manuscript format. This dissertation comprises of two manuscripts that have been combined to satisfy the requirements of the Department of Biomedical and Pharmaceutical Sciences, College of Pharmacy, University of Rhode Island.

Manuscript 1: Introduction to Metal Nanoparticles: Application in Pharmaceutical Sciences

This manuscript is being prepared for submission to *Materials Chemistry and Physics.*

Manuscript 2: Enhanced Cellular Clearance of Gold Nanoparticles by Copper Sulfide Nanoparticles Through ATP7B as Transporter

This manuscript is being prepared for submission to *ACS Nano*.

TABLE OF CONTENTS

LIST OF FIGURES

MANUSCRIPT 1

MANUSCRIPT 2

blocking with 10% goat-serum for 30 min at room temperature. The cells were incubated with RbxMs Anti-Cytokeratin 18 Mab (Abcam, 1:100) at 4^{o}C overnight. After PBS washing for three times, the cells were stained with Alexa Fluor 555 goat anti-rabbit IgG (1:500) for 1 h at room temperature. After PBS washing for 3 times, the cell nuclei were counterstained with DAPI. Mouse primary kupffer cells were separated through incubation with 10 uL phycoerythrin(PE)-conjugated anti-F4/80 antibody in the dark for 15 min at 4oC, and washed with 1 mL BPE. The cell pellet was then resuspended in 100 uL BPE and incubated with 20 uL anti-PE microbeads (Miltenyi Biotec) in the dark for 15 min at 4 ^{o}C. The cells were seeded on rat-tail type I collagen (Corning, Product #354236) coated coverslips. After 24 h, the cells were fixed with cold acetone for 5 min. After PBS washing for three times, the cell nuclei were counterstained with DAPI. Bar, 50 μm. (B), Endocytosis and exocytosis of Cu by primarily cultured mouse hepatocytes and kupffer cells. Hepatocytes and kupffer cells were incubated with PEG-HCuSNPs (10 μg/mL) pretreated with intact mouse serum for 1 h followed by replacement with fresh media. Cu concentrations in lysate of hepatocytes and kupffer cells were analyzed. Data are presented as mean ± standard deviation (n = 4). (C-E), TEM of hepatocytes at 1 h following incubation with PEG-HCuSNPs in the presence of 2% intact mouse serum. (C), Distribution of CuS nanoparticles in cells. White arrows, late endosomes; Arrowheads, lysosomes; Pink arrows, decomposed CuS nanoparticles in the late endosome; Orange arrows, decomposed CuS nanoparticles in vacuoles inside the late endosome. (D), Exocytosis of CuS nanoparticles. Arrowheads, nanoparticles in exosomes with decomposed nanostructures; Arrows, an exosome being released directly from the cytoplasm

Figure 5. Western blott analysis of complement C3 (A) and C5 (B) in nanoparticle-adsorbed proteins. PEG-HAuNS or PEG-HCuSNPs were incubated for 30 minutes with 10% freshly collected mouse serum from two mice, followed by centrifugation to separate nanoparticles (pellet) from the serum (supernatant). Samples were loaded for Western blotting analysis using rat anti-mouse C3 mAb or rat anti-mouse C5a mAb as first antibody. Lanes (1) and (7), supernatant from PEG-HAuNS-incubated serum; Lanes (2) and (8), PEG-HAuNS-bound protein (pellet); Lanes (3) and (9), supernatant from PEG-HCuSNPs-incubated serum; Lanes (4) and (10), PEG-HCuSNPs-bound protein (pellet); Lane (6), diluted freshly collected mouse serum; Lane (5), protein ladder.…….…...75

Figure 6. The primarily isolated mouse hepatocyte could form the bile canaliculi and functional to excrete the HCuSNPs after two days incubation (A), Confocal image of bile canaliculi after 2 days primarily isolated mouse hepatocyte incubation. Mouse primary hepatocytes were seeded in 35mm petri dish pre-coated with rat-tail type I collagen and incubated for 48 hours. Cells were washed twice with 1ml pre-warmed HBSS (with Ca^{2+}/Mg^{2+}). Then, 1 ml of pre-warmed HBSS (with Ca^{2+}/Mg^{2+}) containing 5μM CDFDA was added and incubated cells for 20 minutes in a 37°C incubator with 5% CO_2. At the end of the incubation, aspirated medium and washed cells twice with 1 ml pre-warmed HBSS (with Ca^{2+}/Mg^{2+}) buffer. Assess cell

LIST OF TABLES

MANUSCRIPT 2

LIST OF ABBREVIATION

Surface Plasmon Resonance (SPR)

Near-infrared (NIR)

Polyethylene glycol (PEG)

Reactive oxygen species (ROS)

PEGylated hollow CuS nanoparticles (PEG-HCuSNPs)

Polyvinylpyrrolidone (PVP)

Localized surface plasmon resonances (LSPRs)

Resonance imaging (MRI)

Computed tomography (CT)

Positron-emission tomography (PET)

Single-photon-emission computed tomography (SPECT)

Superparamagnetic ion oxide nanoparticles (SPIO)

Antibodies conjugated to magnetic nanoparticles (Ab-MNPs)

Bone morphogenic proteins (BMPs)

Adipose-derived stem cells (ADSCs)

Physiologically based pharmacokinetic (PBPK)

Absorption, distribution, metabolism, and excretion (ADME)

Organization for Economic Cooperation and Development (OECD)

Registration, Evaluation and Authorisation of Chemicals (REACH)

Quantitative structure–activity relationship (QSAR)

Gastrointestinal (GI)

5 (and 6)-carboxy-2',7'-dichlorofluorescein (CDFDA)

Reticuloendothelial system (RES)

PEGylated hollow CuS nanoparticles (PEG-HCuSNPs)

Transmission electron microscopy (TEM)

Institutional Animal Care and Use Committee (IACUC)

Matrix-assisted laser desorption ionization-time-of-flight imaging mass spectrometry (MALDI-TOF)

Inductively coupled plasma mass spectrometry (ICP-MS)

MANUSCRIPT 1

This manuscript is being prepared for submission to *Materials Chemistry and Physics*.

Introduction to Metal Nanoparticles: Application in Pharmaceutical Sciences

Xiaodong Wang,[a] Wei Lu, [a,b] Bingfang Yan. [a]*

a. Department of Biomedical and Pharmaceutical Sciences, College of Pharmacy, The University of Rhode Island, Kingston, Rhode Island 02881, United States

b. Key Laboratory of Smart Drug Delivery, Ministry of Education, & State Key Laboratory of Molecular Engineering of Polymers, School of Pharmacy, Fudan University, 826 Zhangheng Road, Shanghai 201203, China.

*Corresponding author: Department of Biomedical and Pharmaceutical Sciences, College of Pharmacy, The University of Rhode Island, 7 Greenhouse Road, Kingston, Rhode Island 02881, USA. Phone: +1-401-874-5032. E-mail: byan@uri.edu

KEYWORDS: metal nanoparticle, pharmaceutical sciences.

Abstract

Nanoparticles are small (<100nm) with high surface area to volume ratio, which imparts many advantages such as easy surface modification and high loading volume. Over the past few decades, metallic nanoparticles have emerged as important players in the biomedical application field. They are widely used as high contrast agents in bioimaging such as MRI, and serve as efficient delivery tools for gene therapy, cancer drug delivery and big size biolabeling molecule transportation. Metallic nanoparticles have represented an extraordinary platform for a distinct array of biological uses. This review details the methods for synthesizing the metal nanoparticles, their application in the biomedical field and their pharmacokinetic and toxicity issues.

1. Introduction

Metal nanoparticles were widely used in making paints and glass panel staining long before their properties have been discovered and understood. [1] Precious metal, such as gold, has extensively been used and played crucial roles in ancient China and Arabic medicine to treat rheumatoid arthritis. [2] Colloidal gold has been used to treat alcoholism in the United States since the nineteenth century. [3] Silver, another noble metal, also has been used as eye drops to prevent gonorrhea in newborns from 1880s to the late 1900s [4]. After the successful synthesis of the platinum compound in the 1960s, cisplatin has become one of the most extensively used anticancer drugs, especially in the treatment of ovarian and testicular cancers. [5, 6] Since then, a plethora of literatures have been published to explain the recent advances in nanotechnology [7- 11]. Nanoparticles demonstrate a useful platform with enormous potential in cancer therapy and other biological applications. [12] Some noble metal nanoparticles including gold have received increased attention from the scientific community due to their distinctive properties and wide-range of applications. The major current and most promising applications of metal nanoparticles include *in vivo* and *in vivo* imaging, diagnostics, therapeutics, drug carrier and delivery, biomaterials, biosensor and tissue engineering (Figure 1) [10].

Figure 1. Application of metal nanoparticles in various biomedical fields

2. Methods for Preparation of Metal Nanoparticles

In order to prepare metallic nanoparticles with the preferred sizes and morphologies, many methods including physical, chemical and green biological approaches are used (some important methods are listed in Figure 2). Every method has its advantages and drawbacks, which include using toxic solvents, expensive materials, intensive labor and many others.

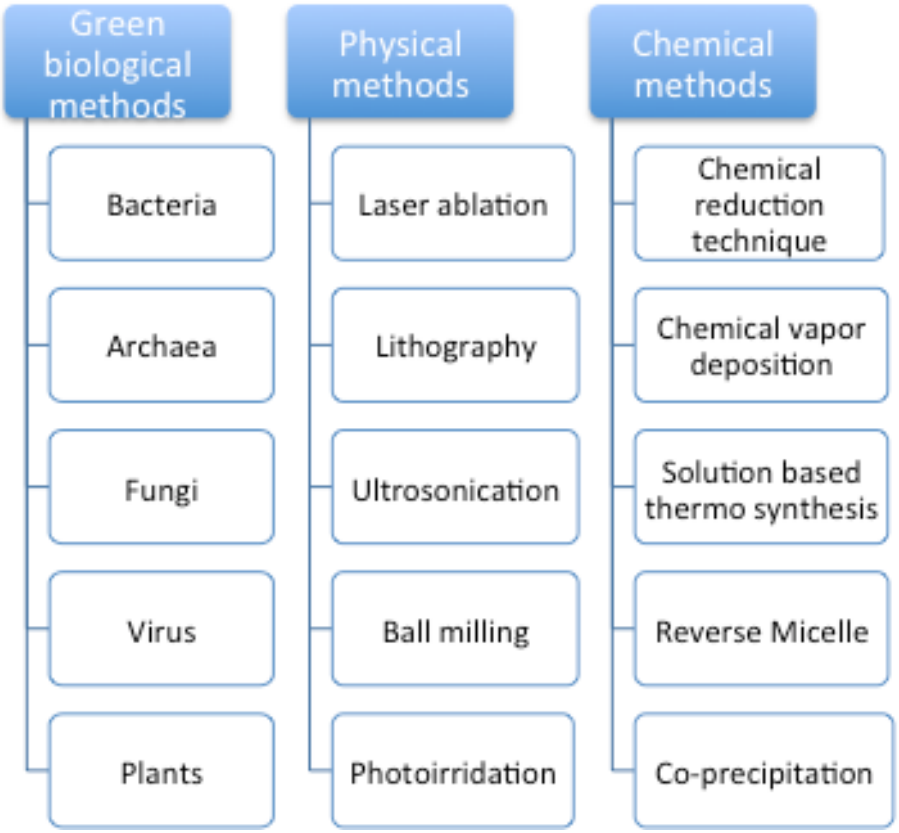

Figure 2. Examples of physical, chemical and green biological methods for metallic nanoparticle preparation

2.1 Chemical and Physical Methods

In chemical reduction method, different kinds of reducing agents including sodium borohydride, ascorbate, sodium citrate, dimethylformamide, etc., are used to reduce metal ions. [13-15] It is very important to use stabilizing agents throughout the reduction process to protect the metallic nanoparticles from agglomeration and sedimentation. [16] Polymeric compounds such as polyvinylpyrrolidone (PVP), polyethylene glycol (PEG), and polymethacrylic acid, which comprise thiols, amines, alcohols groups interact with particle surfaces to stabilize the final nanoparticles and prevent them from growing and losing their surface properties.

High-energy mechanical milling is a very effective physical method for metallic nanoparticle synthesis. Fe−Cu nanoparticles have been successfully synthesized using a ball-milling process that utilizes $FeCl_3$ and $CuCl_2$ [17]. Huang and Yang reported that silver nanoparticles were prepared by using UV- initiated photoreduction of silver nitrate in inorganic lay suspension at room temperature. [18] Metallic nanoparticles prepared in the two-phase aqueous-organic system was reported for silver nanoparticle synthesis. [19] The major disadvantage of this method is the tremendous toxic organic solvents. Therefore, large amounts of surfactants and organic solvents need to be separated and removed from the nanoparticles. In the electrochemical synthetic method, the homogeneity and particle length of a nanoparticle is easier to be controlled by modifying the composition of the electrolytic solution and adjusting the electrolysis parameters. In one study, spherical silver nanoparticles with narrow length distributions were prepared by this method, and poly *N*-vinylpyrrolidone was used to protect nanoparticles from agglomeration [20].

2.2 Green Biological Methods

There is always a demand for using green biological methods to synthesize metallic nanoparticles. Advantages of these methods include i) non-toxic and inexpensive materials and solvents ii) less hazardous chemical process and waste iii) cost-effective and iv) procedures can be done at room temperature. However, disadvantages include i) limitations to repeat and scale up the massive production ii) more studies are needed to elucidate the exact synthesis mechanism and iii) difficulty producing the appropriate size and morphologies of the nanoparticles.

Instead of organic solvents, polysaccharides (e.g., corn starch, dextran, cellulose) and chitosan have been used for the green preparation of metallic nanoparticles. It is reported that silver NPs were synthesized using polysaccharides as capping agents and water as an eco-friendly solvent [21]. Polysaccharides have hydroxyl groups and a hemiacetal-reducing end that can be used as a reducer. The oxidation of hydroxyl groups in polysaccharides to carbonyl groups performs a crucial role in reducing gold salts to form nanoparticles. Furthermore, the hemiacetal-reducing end of polysaccharides can be used to stabilize metallic nanoparticles and prevent sedimentation [22, 23]. For example, starch-stabilized and glucose-reduced silver NPs with a mean diameter of 5.3 nm were prepared through the incubation of silver salt with starch-stabilization and glucose-reduction at 40 °C for 20 h. [24].

3. Application of Metallic Nanoparticles

Nanoparticles have different shapes and a large surface to volume ratio. These two advantages impart nanoparticles with the capability to actively interact with proteins and cell membranes. Metal nanoparticles with localized surface plasmon resonances (LSPRs) property offer more advanced ways for disease diagnosis and treatments based on the resonant oscillation of electrons at the surface of the metal. Besides nanoparticles with LSPRs property, other heavy metals and quantum dots also have the potential to be used in diagnostic tests and as cell trackers and contrasting agents. [25] Moreover, some of the metallic nanoparticles, such as gold and copper have shown the extraordinary ability to be used in drug delivery and photothermal therapy [26]. The application of metallic nanoparticles can be sorted into three

interrelated areas: diagnosis, drug delivery and regenerative therapies.

3.1 Metallic Nanoparticles in Diagnostics

The application of metallic nanoparticles in diagnostics can be further categorized into i) *in vitro* diagnostic tool by using nanoparticles as a probe for disease-related biomarker detection and ii) *in vivo* imaging for *in situ* disease monitoring.

Metallic nanoparticles made with semiconductor material have proved to better bioprobes compared to conventional fluorescent probes. They are more photochemically stable and have a more controllable symmetric emission spectrum. [27] Gold nanoparticles have been used as a color marker for rapid pregnancy testing since the 1980s. Collagen has been used as a biocoating to increase the biocompatibility and improve the interaction with biomolecules, while also reducing the degradation rate of nanoparticles. Metallic nanoparticles with localized surface plasmon resonance (SPR) properties exhibit enhanced scattering and absorption light at specific light wavelengths. [28] Gold nanoparticles have very good SPR property. Within a protein-rich environment, the surface of gold nanoparticles can be conjugated with different proteins. This binding process will increase the size of gold nanoparticles and shift the SPR towards the longer wavelengths. This process can be used for protein qualification and quantification. [29] As an application, specific antibody-coated gold nanoparticles are applied to detect antigen at extremely low concentrations in the nanomolar range, which cannot be achieved with current diagnostic tools. This will identify subtypes of cancer earlier and promote the

diagnosis and prognosis of cancers.[29]

In vivo imaging, such as magnetic resonance imaging (MRI), computed tomography (CT), positron-emission tomography (PET), and single-photon-emission computed tomography (SPECT) are widely used imaging instruments for monitoring and diagnosing complex diseases, including cancer metastasis, and for monitoring the different stages of cardiovascular disease. [30] Gold nanoparticles are superparamagnetic compared to its bulk counterparts. It can be used as an MRI contrast agent. Also, gold nanoparticles are high-resolution candidates for X-ray contrast agents. They are reported to monitor the tumor-related microvasculature progress in cancer metastasis. The leaky capillaries produced during metastasis allow the gold nanoparticles to invade into the extravascular region of the newly malignant tissue. [31]. Also, Zuo and his colleagues reported that the iron oxide nanoparticles loaded with iRGD peptide nanocomplex can be successfully used as ultrasensitive MRI contrast agent for the detection of pancreatic cancer. [32]

3.2 Metallic Nanoparticles in Advanced Drug Delivery

Drug delivery systems are designed to bring therapeutic agents to the target site efficiently with minimum toxicity to healthy surrounding tissue. [33, 34] In regards to the application of metal nanoparticles as a drug delivery system, they have to overcome the reticuloendothelial system barriers such as macrophages. The phagocytic removal of nanoparticles could limit the range of their application as delivery tools in human biology and medicine. However, these nanocarriers surface can be modified with polyethylene glycol to the surface. This coating will form a

hydrated layer between proteins and nanoparticles, which reduces the risk of opsonization by serum proteins and internalization of nanoparticles by phagocytes. [35] Conventionally, chemotherapy target cancer cells by stopping cell division and inducing cell apoptosis/necrosis. The healthy cells, however, will also be impacted by chemotherapy, and as a result, the quality of life for patients is impaired significantly. In this context, highly selective targeted delivery of chemotherapy is a key to efficient cancer therapy and improving cancer patients' quality of life. There are two strategies used to reduce toxicity to healthy tissue during the targeted delivery of metal nanoparticles to the cancer site: active and passive.

In active targeting, the surfaces of metal nanoparticles are conjugated with ligands, whose receptors are expressed on the tumor cell surface. The high affinity binding of the ligand and receptor will enhance the rapid internalization of the nanoparticles. In passive targeting, blood vessels in tumor tissue have a high degree of porosity because they lack angiotensin II receptors and pericyte coverage within vessels, and this leads to the enhanced permeability and retention effect (EPR) [36]. The EPR effect allows nanoparticles conjugated with anticancer therapeutics to penetrate into the extracellular tumor matrix from the tumor capillaries [37].

Besides being applied as drug delivery tools, nanoparticles are also emerging as relatively simple and effective vectors for gene delivery due to their wide-range of sizes, easier surface modification, higher loading capacity and better biocompatibility. [38] Viral and non-viral gene transfer techniques have been widely used for gene transfer. These methods, however, have innate drawbacks such as less efficient transfer, higher toxicity and higher immunogenicity that limit their applications. As a

gene delivery tool, metal nanoparticles protect DNA from degradation by nucleases and facilitate the internalization of DNA into the nucleus. Guo and his colleagues reported the feasibility of applying the charge-reversal functional gold nanoparticles as a means of improving the siRNA delivery efficiency, and the final knockdown efficiency was better than that of commercial Lipofectamine 2000. [39] Other nanoparticles such as ion oxide, carbon nanotubes, magnesium phosphate and other metal nanoparticles are also candidates for DNA delivery vehicles. [40] Polyethyleneimine (PEI)-PEG-chitosan copolymer coated superparamagnetic ion oxide nanoparticles (SPIO) were also reported to deliver the plasmid DNA into the nucleus successfully and safely. [41, 42]

3.3 Metal Nanoparticles in Regenerative Therapies

Using stem cells to regenerate tissues and organs have revolutionized the current techniques in organ transplantations. This better developed technique will be a promising option to meet the needs of organ transplantation and save more lives. Regenerative therapies using nanoparticles form a new area combining nanotechnology and engineering. Tissues and organs developed by using stem cells from an individual can be cultured *in vitro* and then transplanted back into the same individual using a scaffold that the body's immune system cannot distinguish to avoid rejection [43,44]. Superparamagnetic ion oxide nanoparticles (SPIO) as described above, are not only used to improve the safety and efficiency of gene delivery, but also used to improve the detection sensitivity for MRI imaging. [45] The SPIO used for MRI does not alter the function, proliferation or differentiation of hematopoietic stem

cells (HSC) and mesenchymal stem cells (MSC) while being nontoxic and biodegradable. [46]

Magnetic nanoparticles can be conjugated with specific antibodies for selectively targeting stem cells, which express specific receptors for antibodies. The stem cells then can be isolated and recovered by applying a magnetic field. Using this "fishing technique", Lui et al. reported the successful extraction and isolation of stem/progenitor cells from the brain of rats by using antibodies conjugated to magnetic nanoparticles (Ab-MNPs). These magnetically isolated stem cells are functional and can be differentiated into different types of cells *in vitro*. This technique of nanoparticle-mediated isolation and retransplantation of stem cells is now well adopted for the treatment of leukemia and several cardiac diseases. [47]

Recently, immense attention has been placed on metallic nanoparticles as scaffolds in bone regeneration. [48] The nanostructure size of bones is around 1 to 100 nm. Therefore, coating the artificial implants with nano-scaled materials before transplantation would increase the biocompatibility and reduce graft rejection by the immune system. Some bone morphogenic proteins (BMPs) have been reported to play a crucial role in bone regeneration, especially in periodontal tissue [49]. They however cannot be used directly due to inherent limitations such as local inflammation. In recent years, gold nanoparticles have been used as a new generation of osteogenic agents for bone. Heo and colleagues have developed a new approach for bone tissue regeneration utilizing biodegradable hydrogel loaded with gold nanoparticles (GNPs). The *in vitro* results show that GNPs loaded with hydrogels promote the differentiation of human adipose-derived stem cells (ADSCs) into osteoblast cells. Moreover, the *in*

vivo results show that the hydrogel nanostructure has a significant influence on the new bone formation and can be useful for bone tissue engineering. [50]

4. Pharmacokinetics and Toxicity of Metal Nanoparticles

Recently, physiologically based pharmacokinetic (PBPK) modeling is widely used by researchers to investigate the absorption, distribution, metabolism, and excretion (ADME) of metal nanoparticles. The Organization for Economic Cooperation and Development (OECD) and the new European Union regulatory framework REACH (Registration, Evaluation and Authorization of Chemicals) have published guidance, standards and quantitative tools for metal nanoparticle toxicity tests, quantitative structure–activity relationship (QSAR) and PBPK models. [51] The toxicological aspects of metal nanoparticles highly depend on its administration routes, concentrations and exposure times. Exposure to high doses and high levels of metal nanoparticles always induce toxicity. [52] Different routes of administration lead to different organ accumulation of metal nanoparticles. Also, the blood supply amount also plays an important role. After oral administration, nanoparticles may be digested by gastrointestinal (GI) tract and excreted in feces. [53]. If the nanoparticles are administrated through intraperitoneal (IP) and other injection routes, the nanoparticles will be mostly absorbed into lymph nodes [54]. No matter which route nanoparticles are administrated, most of them will be trapped in the reticuloendothelial system (RES), especially in the liver and spleen. This can be reduced or decreased however by coating the surface of nanoparticles with hydrophilic polymers such as PEG. [55]. In addition to the liver and spleen, metal nanoparticles are also found in the

GI tract, kidney, lung, heart, and brain. Metal nanoparticles also encounter different proteins including the complement system in the blood. After coating with these hydrophilic polymers, some of the metal nanoparticles such as copper sulfide can be metabolized and excreted in the urine and feces. [56] Although researchers have increased focus on the toxicity and applications of metal nanoparticles, studies on the toxicity and adverse effects of metal nanoparticles are still in the early stages. The toxicity of nanoparticles is largely based on the physiochemical properties such as composition, morphology, shape, size and surface coatings. [57] These properties could be attributed to the excessive presence of intracellular reactive oxygen species (ROS) and the subsequent activation of pro-inflammatory genes. [58] The toxicity of metal nanoparticle also depends on the cell types used in the studies. Patra et al. reported that 33 nm citrate-capped gold nanospheres induced apoptosis in the human carcinoma lung cell line A549. However, the two other cell lines tested, BHK21 (baby hamster kidney) and HepG2 (human hepatocellular liver carcinoma), remained unaffected by the same concentrations of gold nanospheres treatment. [59] With our understanding of the metal nanoparticle, it is worth mentioning that the results of the *in vitro* toxicity studies of metal nanoparticles cannot be extrapolated to the *in vivo* toxicity studies or be used for clinical applications directly. In the future, establishing a precise toxicological study platform for evaluating metal nanoparticles in medicine is essential and required for improving its safety on human life.

5. Summary

The recent development of nanotechnology and material sciences has created a

plethora of studies in metal nanoparticles. The results of these studies are widely applicable in our daily lives, especially in the medical field for use in high contrast imaging, drug delivery, and therapeutics. In the future, applications of metal nanotechnology show great promise in improving our health and daily lives. The attractive properties of metal nanoparticles such as their ability to be circulated in the blood and translocated successfully into the nucleus due to their small size also make them very dangerous. Diseases from the exposure to metal nanoparticles may not be diagnosed immediately, but will manifest in the future. Many metal nanoparticles also have low metabolic rates compared to their bulk counterparts. In short, metal nanoparticles will have a huge impact on our lives in the future. Therefore, standards and regulations should be created to protect us from the toxicity and adverse effects of metal nanoparticles.

Reference:

1. Heiligtag, F. J.; Niederberger, M. The fascinating world of nanoparticle research. Mater. Today 2013, 16 (7−8), 262−271.

2. Allardyce, C.S.; Dyson, P.J. Ruthenium in medicine: current clinical uses and future prospects. Platinum Metals Rev. 2001, 45 (2), 62–69.

3. Patra C.R.; Bhattacharya, R.; Mukhopadhyay, D.; Mukherjee, P., Fabrication of Gold Nanoparticles for targeted therapy in pancreatic cancer. Advanced drug delivery reviews. 2010;62(3):346-361. doi:10.1016/j.addr.2009.11.007.

4. Alarcon, E.; Griffith, M.; Udekwu, K.I., 2005, Silver Nanoparticles Applications, Springer International publishing.

5. Reedijk, J. Improved understanding in platinum antitumor chemistry. Chem. Commun.,1996,12 , 801–806.

6. Wong, E.; Giandomenico, C.M., Current status of platinum based antitumor drugs. Chem. Rev. 1999, 99, 2451–2466.

7. Farokhzad, O.C.; Langer, R., Impact of nanotechnology on drug delivery. ACS Nano, 2009, 3 (1), 16–20.

8. Abadeer, N.S.; Murphy, C.J. Recent progress in cancer thermal therapy using gold nanoparticles. J. Phys. Chem. C, 2016, 120 (9), 4691–4716.

9. Dreaden, E.C.; Alkilany, A.M.; Huang, X.; Murphy, C.J.; El-Sayed, M.A., The golden Age: gold nanoparticles for biomedicine. Chem. Soc. Rev., 2012 (41), 2740–2779.

10. Shi, J.; Votruba, A.R.; Farokhzad, O.C.; Langer, R., Nanotechnology in drug delivery and tissue engineering: from discovery to applications. Nano Lett. , 2010, 10, 3223–3230.

11. Kratz, F.; Warnecke, A., Finding the optimal balance: challenges of improving conventional cancer chemotherapy using suitable combinations with nano-sized drug delivery systems. J. Controlled Release, 2012, 164, 221–235.

12. Zou, L; Wang, H; He, B; Zeng, L; Tan, T; Cao, H; He, X; Zhang, Z; Guo, S; Li, Y., Current Approaches of Photothermal Therapy in Treating Cancer Metastasis with Nanotherapeutics. Theranostics 2016; 6(6):762-772.

13. Wiley, B.; Sun, Y.; Mayers, B.; and Xi, Y., Shape-controlled synthesis of metal nanostructures: the case of silver. Chem. Eur. J., 2005, 11, 454–463.

14. Evanoff, D.D.; Chumanov, G., Size-Controlled synthesis of nanoparticles. 2. Measurement of extinction, scattering, and absorption cross sections. J. Phys. Chem. B, 2004, 108, 13957–13962.

15. Merga, G.; Wilson, R.; Lynn, G.; Milosavljevic, B.; Meisel, D., Redox catalysis on “naked” silver nanoparticles. J. Phys. Chem. C, 2007, 111, 12220–12226.

16. Oliveira, M.; Ugarte, D.; Zanchet, D.; Zarbin, A., Influence of synthetic parameters on the size, structure, and stability of dodecanethiol-stabilized silver nanoparticles. J. Colloid Interface Sci., 2005, 292, 429–435.

17. Todaka, Y.; McCormick, P.G.; Tsuchiya, K.; Umemoto, M., Synthesis of Fe-

Cu nanoparticles by mechanochemical processing using a ball mill. Mater. Trans., 2002, 43, 667–673.

18. Huang, H.; Yang, Y., Preparation of silver nanoparticles in inorganic clay suspensions. Compos. Sci. Technol. 2008, 68, issue 14, 2948-2953.

19. Zhang, W.; Qiao, X.; Chen, J.; Synthesis of Nanosilver Colloidal Particles in Water/Oil Microemulsion. Colloids and Surfaces A: Physicochemical and Engineering Aspects, 2007, 299, 22-28.

20. Ma, H.; Yin, B.; Wang, S.; Jiao, Y.; Pan, W.; Huang, S. et al., Synthesis of silver and gold nanoparticles by a novel electrochemical method. ChemPhysChem, 2004, 24, 68–75.

21. Sathishkumar, M.; Sneha, K.; Won, S.W.; Cho, C.W.; Kim, S.; Yun, Y.S., Cinnamon zeylanicum bark extract and powder mediated green synthesis of nano-crystalline silver particles and its bactericidal activity. Colloids Surf., B , 2009, 73 , 332–338.

22. Mata, Y.N.; Torres, E.; Blázquez, M.L.; Ballester, A.; González, F.; Muñoz, J.A., Gold (III) biosorption and bioreduction with the brown alga Fucus vesiculosus. J. Hazard. Mater., 2009, 166 , 612–618.

23. Nadkarni, V.D.; Pervin, A.; Linhardt, R.J., Directional immobilization of heparin onto beaded supports. Anal. Biochem. , 1994, 222, 59–67.

24. Raveendran, P.; Fu, J.; Wallen, S., Completely “green” synthesis and stabilization of metal nanoparticles. J. Am. Chem. Soc., 2003, 125, 13940–

13941.

25. Praetorius, N.P.; Mandal, T.K., Engineered nanoparticles in cancer therapy. Recent Pat. Drug Delivery Formul. , 2007, 1, 37–51.

26. Guo, L.; Yan, D.; Yang, D.; Li, Y.; Wang, X.; and et.al., Combinatorial Photothermal and Immuno Cancer Therapy Using Chitosan-Coated Hollow Copper Sulfide Nanoparticles. ACS Nano, 2014, 8, 6, 5670-5681. DOI: 10.1021/nn5002112

27. Bruchez, M. Jr.; Moronne, M.; Gin, P.; Weiss, S.; Alivisatos, A.P., Semiconductor nanocrystals as fluorescent biological labels. Sci. New Ser., 1998, 281 (5385), 2013–2016. doi: 10.1126/science.281.5385.2013.

28. Huang, X.; El-Sayeda, M., Gold nanoparticles: Optical properties and implementations in cancer diagnosis and photothermal therapy. Journal of Advanced Research. 2010, 1,1, 13-28.

29. Nietzold, C.; Lisdat, F., Fast protein detection using absorption properties of gold nanoparticles. Analyst, 2012, 137 , 2821–2826.

30. Mao, J.; Zhang, J.; Nie, M.; Lu, S.; Wu, X., Diabetes insipidus as the first symptom caused by lung cancer metastasis to the pituitary glands: Clinical presentations, diagnosis, and management. J Postgrad Med 2011;57:302-6.

31. Chien, CC.; Chen, H.H.; Lai, S.F.; et al., Gold nanoparticles as high-resolution X-ray imaging contrast agents for the analysis of tumor-related micro-vasculature. Journal of Nanobiotechnology. 2012;10:10. doi:10.1186/1477-

3155-10-10.

32. Zuo, H.; Yao, W.; Chen, T.; et al., The Effect of Superparamagnetic Iron Oxide with iRGD Peptide on the Labeling of Pancreatic Cancer Cells In Vitro: A Preliminary Study, BioMed Research International, vol. 2014, Article ID 852352, 8 pages, 2014. doi:10.1155/2014/852352

33. Pramanik, A.; Laha, D.; Pramanik, P.; Karmakar, P., A novel drug "copper acetylacetonate" loaded in folic acid-tagged chitosan nanoparticle for efficient cancer cell targeting. J. Drug Targeting, 2014, 22 (1), 23–33.

34. Kang, L.; Gao, Z.; Huang, W.; Jin, M.; Wang, Q., Nanocarrier-mediated co-delivery of chemotherapeutic drugs and gene agents for cancer treatment. Acta Pharmaceutica Sinica B. 2015;5(3):169-175. doi:10.1016/j.apsb.2015.03.001.

35. Lim, E.K.; Jang, E.; Lee, K.; Haam, S.; Huh, Y.M., Delivery of Cancer Therapeutics Using Nanotechnology. Pharmaceutics 2013, 5, 294-317.

36. Kobayashi, H; Watanabe, R.; Choyke, P.L., Improving Conventional Enhanced Permeability and Retention (EPR) Effects; What Is the Appropriate Target? Theranostics. 2014;4(1):81-89. doi:10.7150/thno.7193.

37. Danhiera, F.; Ucakar, B.; Magotteaux, N.; Brewster, M.E.; Preat, V., Active and passive tumor targeting of a novel poorly soluble cyclin dependent kinase inhibitor, JNJ-7706621. Int. J. Pharm., 2010, 392 , 20–28.

38. Rai, M.; Deshmukh, S.; Gade, A.; Elsalam, K.A., Strategic nanoparticle-mediated gene transfer in plants and animals – a novel approach. Curr.

Nanosci. , 2014, 8, 170–179. doi: 10.2174/1573413711208010170.

39. Guo, S.; Huang, Y.; Jiang, Q.; Sun, Y.; et, al., Enhanced Gene Delivery and siRNA Silencing by Gold Nanoparticles Coated with Charge-Reversal Polyelectrolyte. ACS Nano, 2010, 4 (9), pp 5505–5511. DOI: 10.1021/nn101638u.

40. Sokolova, V.; Epple, M., Inorganic nanoparticles as a carrier for nucleic acid into cells. Angew. Chem. Int. Ed., 2008, 47, 1382–1395.

41. Kievit, F.M.; Veiseh, O.; Bhattarai, N., et al., PEI-PEG-Chitosan Copolymer Coated Iron Oxide Nanoparticles for Safe Gene Delivery: synthesis, complexation, and transfection. Adv Funct Mater. 2009; 19:2244–2251.

42. Veiseh, O.; Kievit, F.M.; Gunn, J.W.; et al., A ligand-mediated nanovector for targeted gene delivery and transfection in cancer cells. Biomaterials. 2009; 30:649–657.

43. Hofmann, M.C., Stem Cells and Nanomaterials. Advances in experimental medicine and biology. 2014;811:255-275. doi:10.1007/978-94-017-8739-0_13.

44. Barnes, C.P.; Sell, S.A.; Boland, E.D.; Simpson, D.G.; Bowlin, G.L., Nanofiber technology: designing the next generation of tissue engineering scaffolds. Adv. Drug Delivery Rev., 2007, 10 , 1413–1433.

45. Corot, C.; Warlin, D., Superparamagnetic iron oxide nanoparticles for MRI: contrast media pharmaceutical company R&D perspective. WIREs Nanomed Nanobiotechnol 2013. doi: 10.1002/wnan.1225.

46. Arbab, A.S.; Yocum, G.T.; Rad, A.M; Khakoo, A.Y.; Fellowes, V.; Read, E.J.; Frank, J.A., Labeling of cells with ferumoxides–protamine sulfate complexes does not inhibit function or differentiation capacity of hematopoietic or mesenchymal stem cells. NMR Biomed. 2005; 18:553–559.

47. Lui, C.N.; Tsui, Y.P.; Ho, A.S.; Shum, D.K.; Chan, Y.S.; Wu, C.T.; et al., Neural stem cells harvested from live brains by antibody-conjugated magnetic nanoparticles. Angew. Chem. Int. Ed., 2013, 52 , 12298–12302.

48. Yi, H.; Ur, R. F.; Zhao, C.; Liu, B.; He, N., Recent advances in nano scaffolds for bone repair. Bone Research. 2016;4:16050 doi:10.1038/boneres.2016.50

49. Rao, S.M.; Ugale, G.M.; Warad, S.B., Bone Morphogenetic Proteins: Periodontal Regeneration. North American Journal of Medical Sciences. 2013;5(3):161-168. doi:10.4103/1947-2714.109175.

50. Heo, N.D.; Ko, W.K., Bae, M.S; et, al., Enhanced bone regeneration with a gold nanoparticle–hydrogel complex. J. Mater. Chem. B, 2014,2, 1584-1593.

51. Seaton, A.; Tran, L.; Aitken, R.; Donaldson, K., Nanoparticles, human health hazard and regulation. Journal of the Royal Society Interface. 2010;7(Suppl 1):S119-S129. doi:10.1098/rsif.2009.0252.focus.

52. Holgate, S.T. Exposure, uptake, distribution and toxicity of nanomaterials in humans. J. Biomed. Nanotechnol. , 2010, 6, 1–19.

53. Yun, Y.; Cho, Y.W.; Park, K., Nanoparticles for oral delivery: Targeted nanoparticles with peptidic ligands for oral protein delivery. Advanced drug

delivery reviews. 2013;65(6):822-832. doi:10.1016/j.addr.2012.10.007.

54. Kim, J.Y; Cao, L.; Shvartsman, D.; Silva, E.A.; Mooney, D.J., Targeted Delivery of Nanoparticles to Ischemic Muscle for Imaging and Therapeutic Angiogenesis. Nano Lett., 2011, 11 (2), pp 694–700. DOI: 10.1021/nl103812a.

55. Guo, L.R.; Panderi, I.; Yan, D.D.; Szulak, K.; Li, Y.J.; et. al., A Comparative Study of Hollow Copper Sulfide Nanoparticles and Hollow Gold Nanospheres on Degradability and Toxicity. ACS Nano, 2013, 7 (10), 8780–8793. DOI: 10.1021/nn403202w.

56. Ray, P.C.; Yu, H.; Fu, P.P., Toxicity and Environmental Risks of Nanomaterials: Challenges and Future Needs. Journal of environmental science and health Part C, Environmental carcinogenesis & ecotoxicology reviews. 2009;27(1):1-35. doi:10.1080/10590500802708267.

57. Nita, M.; Grzybowski, A. The Role of the Reactive Oxygen Species and Oxidative Stress in the Pathomechanism of the Age-Related Ocular Diseases and Other Pathologies of the Anterior and Posterior Eye Segments in Adults. Oxidative Medicine and Cellular Longevity. 2016;2016:3164734. doi:10.1155/2016/3164734.

58. Patra, H.K.; Banerjee, S.; Chaudhuri.; Lahiri, P.; Dasgupta, A.K., Cell-selective response to gold nanoparticles. Nanomedicine 2007;3:111–119.

This manuscript is being prepared for submission to ACS Nano.

Enhanced Cellular Clearance of Gold Nanoparticles by Copper Sulfide Nanoparticles Through ATP7B as Transporter

Xiaodong Wang,[‡] Liangran Guo,[‡,] Yi-Tzai Chen,[‡,] Yuan Chen,[‡,] Yixin Chen,[‡] Bingfang Yan,[‡] Wei Lu[†,‡,*]

[†]Department of Pharmaceutics, School of Pharmacy, Key Laboratory of Smart Drug Delivery, Ministry of Education, & State Key Laboratory of Molecular Engineering of Polymers, Fudan University, Shanghai 201203, China; [‡]Department of Biomedical and Pharmaceutical Sciences, College of Pharmacy, The University of Rhode Island, Kingston, Rhode Island 02881, United States.

*Corresponding author: Department of Pharmaceutics, School of Pharmacy, Key Laboratory of Smart Drug Delivery, Ministry of Education, & State Key Laboratory of Molecular Engineering of Polymers, Fudan University, 826 Zhangheng Road, Shanghai 201203, China. Phone: +86-21-51980185. Fax: +86-21-51980184. E-mail: wlu@fudan.edu.cn

ABSTRACT

Copper sulfide (CuS) nanoparticles show great potential in therapeutic and diagnostic applications. Gold nanoparticles with bioinert properties have great advantages in the photothermal transaction; however, gold nanoparticles are non-biodegradable, raising concerns regarding their long-term metabolism and safety. Clinical translation of these nanoparticles requires sufficient understanding of their metabolic process *in vitro and in vivo*. Here, we use pegylated hollow CuS nanoparticles (PEG-HCuSNPs) of ~70 nm in diameter as models to elucidate their highly efficient metabolic trafficking in mouse liver and primarily cultured human and mouse hepatocytes. Traverse of Cu-ATPase ATP7B to the nanoparticle-loaded late endosomes/lysosomes, as well as increased ATP7B expression both in the cytosol and on the membrane at one hour following PEG-HCuSNPs injection, show efficient removal of excess Cu ions by hepatocytes to transfer content into bile canaliculi through exocytosis. With this finding, we conjugated gold and copper nanoparticles and found that copper nanoparticles would facilitate the excretion of gold nanoparticles through the transporter ATP7B. Primarily cultured human and mouse hepatocytes exhibit much higher efficiency in terms of exocytosis of PEG-CuSNPs-Au than Au alone, which is similar to the results found in animal bile excretion study. These findings reveal that the high metabolic rate of the systemically administered Cu in the liver could facilitate the excretion of gold nanoparticles much more efficiently than gold administrated alone.

KEY WORDS: Copper sulfide nanoparticles, Au nanoparticles, Metabolism, Hepatocyte, ATP7B

Semiconductor copper sulfide (CuS) nanoparticles, a class of new nanomaterials, have been widely reported for their biomedical applications in recent years. The intriguing optical and physicochemical properties of CuS nanoparticles endue them with great potential in cancer photothermal ablation therapy,[1-4] drug delivery,[5-7] photoacoustic imaging,[8] nuclear medicine[9-12] and their combinations.[7, 9-16] Although Cu is an essential element in the body, excess free Cu ions in excess are toxic.[17] A recent study has shown that CuS nanoparticles are much less cytotoxic than copper oxide nanoparticles because of the extremely low solubility of CuS.[18] Through histological and biochemical examinations, we found that pegylated hollow CuS nanoparticles (PEG-HCuSNPs) do not induce significant liver toxicity during the 3-month study period.[19] PEG-HCuSNPs exhibit a reversible change in the proteomic profile in liver, offering long-term safety benefit.[19] With the above evidence, we believe that the slow dissociation rate of Cu ions from CuS nanoparticles, along with effective mechanisms of Cu elimination, may allow physiological homeostasis to be reached at an optimized dosing schedule without drastically increased toxicity. Metabolism of CuS nanoparticles, accordingly, is critical to Cu homeostasis and toxicity.

Existing pharmacokinetic analyses have shown that CuS nanoparticles can be metabolized.[11, 19] CuS nanoparticles, if smaller than the effective cut-off size for glomerular filtration (~10 nm), are mainly excreted from the kidney.[11] Ultra-small CuS nanoparticles with hydrodynamic diameters less than 6 nm have minimally nonspecific uptake by the mononuclear phagocyte system and highly efficient clearance via the renal-urinary system.[11] Comparatively, clearance of CuS

nanoparticles larger than 10 nm is slower than that of the ultra-small CuS nanoparticles.[11, 19] We have previously demonstrated that about 67% of the injected dose is eliminated from the liver within one month postinjection of PEG-HCuSNPs of ~70 nm in diameter.[19] Therefore, liver is the major organ metabolizing these relatively "large" CuS nanoparticles.[11, 19] However, the mechanism of hepatic metabolism of CuS nanoparticles remains unknown.

Even though different kinds of gold nanoparticles with bioinert properties have a great advantage in the photothermal transaction and are promising for clinical applications, [20, 21] they are non-biodegradable, raising concerns regarding their long-term metabolism and safety.[22, 24] Tail vein injections of polyethylene glycol (PEG)-coated gold nanoparticles have been reported to induce two phases of toxicity due to inflammation in the liver. The acute phase occurred immediately after administration of nanoparticles. The second phase happened at 7 days when the particles become localized in the tissues, mostly in the liver and spleen after circulation in the blood.[25] Due to the multiple valences of gold, redox reaction of gold within cells can increase the levels of reactive oxygen species, which interferes with the mitochondrial membrane potential. Disturbance of the mitochondrial membrane potential after exposure to gold nanoparticles initiates an apoptotic cascade in cells.[26, 27]

In this study, we use PEG-HCuSNPs as models to investigate their trafficking in hepatocytes and Kupffer cells *in vivo*, and to elucidate their metabolic pathway in mouse liver. It is generally believed that nanoparticles predominantly interact with and are engulfed by cells of the mononuclear phagocyte system, such as Kupffer cells in the liver, once these nanoparticles enter the blood.[28] Distinctively, we find that the

majority of PEG-HCuSNPs in liver accumulate in hepatocytes instead of Kupffer cells following injection. The injected PEG-HCuSNPs undergo fast uptake and subsequent disintegration in the endo-lysosomal compartments of hepatocytes, followed by quick exocytosis into bile canaliculi with the assistance of the Cu-ATPase ATP7B. In contrast, most engulfed PEG-HCuSNPs remain intact in Kupffer cells. Our findings reveal that the hepatocytes play a major role in the metabolism of PEG-HCuSNPs, which is distinct from conventional nanoparticle opsonization by mononuclear phagocyte system, such as Kupffer cells. In comparison, Kupffer cells temporarily store the CuS nanoparticles circulating in the blood, but with limited capacity. The metabolism and excretion of PEG-HCuSNPs in hepatocytes are much faster than that in Kupffer cells. Based on this finding in the study, we further conjugated gold and copper sulfide nanoparticles with different kinds of physiochemical properties to study the excretion of gold. It shows that conjugating copper with gold nanoparticles enhance the *in vivo* excretion of gold nanoparticles to reduce their short and long term toxicity, and reveal that the metabolic pathway of the systemically administered CuS nanoparticles in liver could facilitate the excretion of gold nanoparticles much more efficiently than gold alone.

RESULTS AND DISCUSSION

Fast hepatobiliary excretion of PEG-HCuSNPs through efficient nanoparticle trafficking into the bile canaliculi. To understand how PEG-HCuSNPs were metabolized in the liver, we firstly collected bile samples from gall bladders at different times following intravenous (i.v.) injection of the nanoparticles in BALB/c mice. Transmission electron microscopy (TEM) illustrated that the nanoparticles appeared in bile as early as 15 min after the administration (Fig. 1A). Interestingly, at 1 h post injection, in addition to the intact particles, there were many small nanoparticles with diameters around 10 nm or less (arrowheads). At 4 h post injection, one partially disintegrated PEG-HCuSNP is surrounded by many small CuS crystals (yellow dash circle), suggesting that PEG-HCuSNPs may quickly break down during the process of hepatobiliary excretion. Likewise, bile samples collected at 24 and 48 h postinjection contained both large and small CuS nanoparticles. Noticeably, most large CuS particles appeared to be partially disintegrated. We next centrifuged the bile samples to separate the pellet (large and small CuS nanoparticles) from the supernatant (Cu ions) for quantitative analysis of Cu. Figure 1B delineate a continuous hepatobiliary excretion of Cu in both particulate and ionic forms within 1 week following i.v. injection of PEG-HCuSNPs. Excretion of CuS particles in gallbladders decreased over time, especially within 2 d postinjection. This could be attributed to the decreased concentration of the CuS nanoparticles in the blood. In comparison, biliary excretion of Cu ions remained relatively steady even after a week post injection.

We looked further into the nanoparticle distribution in mouse hepatocytes *in vivo*. At 1 h post injection, the endo-lysosome loaded with CuS nanoparticles was

found close to the nucleus (Fig. 2A), in which partially disintegrated large particles (blue arrowheads), large particles with solid structures (orange arrowheads) as well as decomposed small dots (green arrowheads) were present. Those large solid particles consisted of highly packed small CuS dots, suggesting that the hollow structures of PEG-HCuSNPs collapsed and the small CuS dots turned into aggregates during degradation. These collapsed CuS nanoparticles were also found in the lysosome close to the bile canaliculus (Fig. 2B, the structure pseudo-colored in light cyan), indicating that the nanoparticle-loaded lysosome was moving toward the apical membrane of hepatocyte for exocytosis. This hypothesis was further supported by the observation of collapsed CuS nanoparticles was found in the bile canaliculi (Figs. 2C). Large solid particles consisted of highly packed small CuS dots, suggesting that the hollow structures of PEG-HCuSNPs collapsed and the small CuS dots turned into aggregates during degradation (Fig. 2D and 2E). These results, correlating with the bile distribution of Cu, indicate that the injected PEG-HCuSNPs underwent fast endocytosis and disintegration in the endo-lysosomal compartments of hepatocytes, followed by quick exocytosis into the bile canaliculi for efficient hepatobiliary excretion.

Additionally after 1 h following i.v. injection of PEG-HCuSNP, Kupffer cells were loaded with HCuSNPs. Lysosomes were found to fuse with the phagosome to form a phagolysosome. (Fig. 2F, Kupffer cells Structures, pseudo-colored in pink). The number of engulfed nanoparticles per vacuole was greater in Kupffer cell than in hepatocytes (~20 nanoparticles in a vacuole in Fig. 2F *vs.* 3~5 incompletely disintegrated nanoparticles in each vacuole in hepatocytes). Unexpectedly, most

nanoparticles in phagosomes remained intact with hollow interior structures. Only a few decomposed small CuS nanoparticles were observed in the phagolysosomes at 24 h postinjection (Fig. 2G, blue arrow head). This finding was different from the TEM results of hepatocytes in which most nanoparticles were disintegrated or were decomposed after 24 h. The intact morphology of the nanoparticles indicates that metabolism of PEG-HCuSNPs in Kupffer cells was slow and minimal although their phagocytosis was fast and efficient.

The swift disintegration of PEG-HCuSNPs may be ascribed to the interaction between the nanoparticles and cellular components, facilitating the dissociation of Cu ions. To prove this hypothesis, we prepared various media to investigate their effects on Cu^{2+} release from PEG-HCuSNPs. As shown in Figure S1A, there was low dissociation of Cu^{2+} dissociated from PEG-HCuSNPs in phosphate buffered saline (PBS) due to the extremely low solubility of CuS.[18] Addition of amino acids to the medium significantly increased Cu^{2+} release, due to the formation of copper/amino acid complexes.[29] Interestingly, in PBS supplemented with cysteine (Cys) or Cys-HCl, the Cu ion concentration at 24 h was lower than at 1 h or 4 h. This was because Cu^{2+} can induce the oxidation of Cys to cystine, thus precipitating the Cu.[30] In addition, glutathione (GSH) or metallothionine, considered to be part of the Cu storage system,[31] enhanced Cu ion dissolution (Fig. S1B). TEM confirmed that with GSH-treatment, PEG-HCuSNPs collapsed and transformed from hollow structures to solid particles with small CuS particle dissociation (Fig. S1C, arrowheads). A similar phenomenon was observed in PEG-HCuSNPs treated with metallothionine (Fig. S1D, arrowheads). Also, media at lysosomal pH (pH 4.9)[32] significantly increased

dissolution of Cu ions compared to the physiological pH (Fig. S1E). These findings supported the finding that cellular components such as amino acids and Cu storage systems interacted with PEG-HCuSNPs to facilitate their dissociation and further release of Cu ions. Acidic lysosomal conditions may also increase Cu dissolution from the particles.

Efficient excretion of PEG-HCuSNPs by hepatocytes and Kupffer cells in mouse liver. Distinct distribution patterns of PEG-HCuSNPs in hepatocytes and Kupffer cells based on the TEM drove us to understand what roles the two types of cells played in the metabolism of PEG-HCuSNPs. We thus investigated their endocytosis and exocytosis *in vitro* by isolating primary hepatocytes and Kupffer cells from mouse liver with high purity.[19, 37, 38] (Fig. 3A) To mimic the *in vivo* condition, we preincubated PEG-HCuSNPs with freshly collected mouse serum before treating the cells for 1 h. After 30 min post endocytosis, primary hepatocytes and the Kupffer cells reached a balance between endo/exocytosis of PEG-HCuSNPs. (Fig. 3B) After 30 min post excretion, intracellular Cu was reduced by 90% compared to baseline, confirming fast exocytosis of Cu by Kupffer cells. The hepatocytes also have high excretion efficiency since Cu was reduced by 92.2% compared to baseline. However, only 0.17% of copper was left in hepatocytes after 90 min post exocytosis versus 2% left in Kupffer cells. These results demonstrate that both hepatocytes and Kupffer cells exerted high excretion efficiency of PEH-HCuSNPs.

TEM of primary cultured mouse hepatocytes incubated with PEG-HCuSNPs in intact mouse serum for 1 h showed that the nanoparticle-loaded late endosomes (Fig. 3C, white arrows) and lysosomes (arrowheads) distributed extensively in the

cytoplasm. The nanoparticles in lysosomal compartments predominantly disintegrated. In late endosomes with multivesicular structures, the nanoparticles also broke down into small dots but with smaller amounts (Fig. 3C, white, pink and orange arrows). Some decomposed CuS nanoparticles were in vacuoles inside the late endosome (Fig. 3C, orange arrows), suggesting that decomposition of nanoparticles occurred during early-to-late endosomal maturation. Figure 3D illustrated that the nanoparticles were excreted from hepatocytes through exocytosis. The nanoparticles either collapsed or disintegrated in the exosomes (Fig. 3D, arrowheads). In the exosomes released directly from the plasma membrane, the nanoparticles were indistinguishable because of light electron dense (Fig. 3D, arrows). However, a great number of CuS nanoparticle-loaded vesicles (Fig. 3E, arrows) appeared inside the multivesicular bodies fused to the plasma membrane (Fig. 3E, the enlarged image with yellow margin) and excreted out of the cell (Fig. 3E, the enlarged image with red margin). These findings proved that the decomposed CuS nanoparticles were released from hepatocytes through exocytosis by multivesicular bodies such as late endosomes or lysosomes. The results of the TEM study were similar to the transwell endo/exocytosis study and confirmed that excretion of CuS nanoparticles by hepatocytes occurred via lysosomal trafficking to cytoplasmic membrane and extrusion into the bile canaliculi. The excretion rate of CuS nanoparticles in hepatocytes was comparable to that in Kupffer cells, and less remained in hepatocytes after 90 min post exocytosis.

Trafficking and expression of ATP7B in hepatocytes for Cu extrusion in response to the injected PEG-HCuSNPs. Cu-transporting ATPase ATP7B, which is highly expressed in hepatocytes, is crucial for maintaining Cu homeostasis.[33] Under

basal conditions, it transports Cu into the trans-Golgi network (TGN) for metallation of many essential cuproenzymes or ceruloplasmin. Acute elevation of intracellular copper, on the other hand, triggers ATP7B-dependent Cu sequestration and excretion. ATP7B accumulates Cu and redistributes them from the TGN to late endosome/lysosome compartments, followed by fusion with the apical plasma membrane to extrude Cu ions into bile canaliculi.[33-35] In order to investigate how hepatic ATP7B respond to systemically injected PEG-HCuSNPs, we used fluorescein isothiocyanate (FITC)-PEG_{5K}-SH to label the nanoparticles. The FITC-conjugated PEG-HCuSNPs (PEG-HCuSNPs-FITC) had less than 3.5% cumulative fluorescence released in either acetate buffer (pH 4.9, lysosomal mimic) or PBS containing 10% mouse serum over 24 h incubation (Fig. S2), suggesting the fluorescence labeling was stable enough to track the nanoparticles *in vivo*. Figure 4A illustrated that fluorescence of ATP7B (red) colocalized with fluorescence of the labeled nanoparticles (green) and Rab7 (blue), a marker of late endosome/lysosome structures,[36] in mouse hepatocytes at 1 h after i.v. injection (arrows). This result indicated that ATP7B indeed trafficked to the nanoparticle-loaded vesicular compartments, participating in removal of intra-vesicular Cu.

We wondered whether any changes of cellular expression of ATP7B occurred in hepatocytes. To find out, we isolated primary hepatocytes from BALB/c mice following i.v. injection of PEG-HCuSNPs with our modified two-step collagenase digestion method[19, 37,38] Western blot results showed that at 1 h postinjection levels of ATP7B protein increased by 30% in the cytosol and by 72% on the plasma membrane of hepatocytes compared with basal levels, respectively (Figs. 4B and 4C). This

finding showed that the liver quickly launched endogenous detoxification mechanism in hepatocytes in the presence of high loading of PEG-HCuSNPs. Remarkably, elevation of ATP7B on plasma membrane was substantially more than that in cytosol, indicating that more ATP7B trafficked to the apical side membrane in order to accelerate Cu ion excretion for homeostasis.[33, 39] Nevertheless, the cytoplasmic ATP7B declined to 71% at 4 h and further to 66% at 24 h compared to basal levels, while membrane ATP7B returned to baseline. One possible explanation was that the cellular storage of ATP7B was exhausted and production of ATP7B did not meet its demand. Reduction of ATP7B would decrease the cellular capability of removing Cu in hepatocytes, subsequently raising intracellular Cu ion level and causing potential toxicity. This hypothesis was supported by the mRNA analysis that the Atp7b levels declined to ~50% of baseline at 4 h postinjection (Fig. 4D). However, the mRNA transcription restored at 24 h, indicating that hepatocytes quickly recovered from the toxicity and regained ATP7B productivity. Concomitantly, protein expression of cytoplasmic ATP7B was restored to baseline at 2 d postinjection, which was 1 d after recovery of mRNA transcription (Fig. S3). Our previous study demonstrated a reversible change in the proteomic profile of liver tissues in mice receiving PEG-HCuSNPs through matrix-assisted laser desorption ionization-time-of-flight imaging mass spectrometry (MALDI-TOF).[19] The current results from ATP7B analysis, similar to the previous result with proteomic profiling, confirmed that PEG-HCuSNPs-induced toxicity was transient and reversible at a therapeutic dose of 20 mg/kg of Cu.

Cuillel et al. disclosed the metabolic mechanism of CuO nanoparticles in hepatocytes.[40] The CuO nanoparticles underwent fast dissolution once it is delivered

to endo/lysosomes after endocytosis. The burst release of Cu ions caused destabilization/disruption of lysosomes, resulting in Cu^{2+} overload in the cytoplasm. ATP7B played a key role in binding and removing Cu ions in cytosol.[40] In contrast, because of the extremely low solubility of CuS, dissolution of Cu ions from CuS nanoparticles was slow.[18] Significant amounts of CuS nanoparticles remained undissolved in the endo-lysosomal compartment following endocytosis in hepatocytes (Figs. 1B and 2). Noticeably, ATP7B was bound to the CuS nanoparticles in hepatocytes at 1, 4, or 24 h postinjection by Western blotting analysis (Fig. 4E), suggesting ATP7B participated in sequestering/chelating particulate Cu even before Cu dissolution. Since ATP7B was observed to colocalize with the CuS nanoparticle-loaded endo-lysosomes (Fig. 4A), in addition to transporting cytosolic Cu, ATP7B is thought to cross the endo-lysosome compartment to chelate intra-vesicular Cu, regulating both particulate and ionic Cu excretion into bile canaliculi.

Complement C3-mediated phagocytosis of the blood-circulating PEG-HCuSNPs in Kupffer cells without significant degradation. When nanoparticles enter the blood circulation, the nanoparticle's surface is immediately covered with blood proteins and peptides, forming a protein corona.[41] The composition of the protein corona determines the biological response to nanomaterials, directing further tissue process of nanoparticles. To understand effects of nanoparticle-protein interactions on the metabolism of PEG-HCuSNPs *in vivo*, we collected mouse blood after i.v. injection of the nanoparticles. The nanoparticle-bound proteins were identified by tandem mass spectrometry. Table 1 showed gene ontology classification by the function of the nanoparticle-bound proteins from mouse plasma at 5 min or 1 h

following injection. Compared to the nanoparticle-bound proteins at 5 min, the number of proteins increased significantly in all 20 biological process categories at 1 h, suggesting the formation of the protein corona on the surface of PEG-HCuSNPs despite pegylation of nanoparticles. Classification of these bound proteins further revealed that the three largest classes were the cellular process (383), biological regulation (271) and metabolic process (251) at 1 h postinjection, all related to tissue distribution and metabolism. Prominently, the number of metabolic proteins increased from 6 at 5 min to 251 at 1 h postinjection, a highest 41.8-fold increase among all the investigated classes. This result confirmed that proteins directly related to metabolism were prone to binding to PEG-HCuSNPs in blood circulation, and involving the metabolic process of the nanoparticles.

Characteristic of proteins bound to PEG-HCuSNPs would determine the *in vivo* behavior of the nanoparticles and their biological outcomes.[41, 42] We further identified the 10 most abundant proteins adsorbed to PEG-HCuSNPs from mouse blood at 5 min and 1 h postinjection, respectively (Tables 2 and 3). Complement C3, a central protein in the complement system, was the most abundant protein bound to the nanoparticles at both time points following administration. Remarkably, the abundance of C3 among the adsorbed proteins at 1 h was 15.3 times that at 5 min. This observation suggested that the complement system might play an important role in mediating phagocytosis of PEG-HCuSNPs by macrophages, a phenomenon known as opsonization.[43-45]

Several complement receptors expressed on Kupffer cells and hepatocytes are responsible for the elimination of foreign nanoparticles in liver. Kupffer cells express

the receptors for complement C3b, iC3b and C5a, while hepatocytes express C5a receptors.[46] Complement C3b and iC3b are products of C3 activation, while complement C5a is a fragment of C5. In order to confirm C3-coating on the nanoparticles, we incubated PEG-HCuSNPs with 10% mouse serum followed by centrifugation of the nanoparticles. The nanoparticle-bound proteins were then isolated and analyzed by Western blot. Figure 5A illustrated that C3 and its fragment C3b were apparent on the surface of PEG-HCuSNPs (Lanes 4 and 10). Compared with untreated serum (Fig. 5A, Lane 6), C3 alpha chain and unknown fragments (37~50 kD) were newly generated on the surface of PEG-HCuSNPs (Lanes 4 and 10). In contrast, only C3 was clearly detected in the serum supernatant after incubation with PEG-HCuSNPs (Fig. 5A, Lanes 3 and 9). By comparing Lanes 6, 3 and 4 in Figure 5A, we found that serum C3b was transferred to the surface of PEG-HCuSNPs following incubation. These results revealed that PEG-HCuSNPs significantly adsorbed C3 and C3b in blood circulation and initiated the complement activation cascade to further induce cleavage of C3 and/or C3b on the nanoparticle surface. This was possibly attributed to CuS nanoparticles that might react with or chelate amino acid residues of the adsorbed proteins. Since C3b and iC3b specifically bound to their respective receptors expressed on the surface of Kupffer cells,[43-45] significant uptake of PEG-HCuSNPs by Kupffer cells was expected. In comparison, neither C3 nor its fragmentation was detected on the surface of pegylated hollow gold nanospheres (PEG-HAuNS), indicating that PEG-HAuNS did not adsorb C3 in the blood (Fig. 5A, Lanes 2 and 8). This finding, consistent with other studies, confirmed that pegylation of gold nanoparticles prevented C3-mediated opsonization.[47] Results from Western

blot analysis showed little to no complement C5 detected in PEG-HCuSNPs-bound proteins (Fig. 5B, Lanes 4 and 10). PEG-HAuNS did not adsorb C5 in either mouse (Fig. 5B, Lanes 2 and 8). These results demonstrated that C3-mediated opsonization of PEG-HCuSNPs but not PEG-HAuNS in blood circulation. C5 adsorption on either PEG-HCuSNPs or PEG-HAuNS was negligible.

We next assessed whether the C3-mediated opsonization facilitated phagocytosis by the Kupffer cells. TEM of mouse liver showed PEG-HCuSNPs in phagocytic vacuoles, namely phagosomes (Fig. 2F) were found to fuse with lysosomes to form a phagolysosome. Unexpectedly, most nanoparticles in phagosomes remained intact with hollow interior structures. Only a few decomposed small CuS nanoparticles were observed in the phagolysosomes at 24 h postinjection (Fig. 2G). This finding was distinct from the TEM results of hepatocytes in which most nanoparticles disintegrated or were decomposed at 4 h postinjection. The intact morphology of the nanoparticles indicated that metabolism of PEG-HCuSNPs in Kupffer cells was slow and minimal although their phagocytosis was fast and efficient.

The process of opsonization was thought to rapidly eliminate the blood-circulating nanoparticles (0.05--2 μm in diameter) in which Kupffer cells were the major cell type involved in the liver.[28, 48] Our results supported that significant phagocytosis of PEG-HCuSNPs by Kupffer cells took place through opsonization by nanoparticle-associated complement components such as C3 during the initial period postinjection. When the time elapsed, the cellular Cu levels gradually decreased in Kupffer cells. However, TEM results clearly showed that the phagocytized PEG-HCuSNPs remained intact with a little degradation during 1 d of the investigation (Fig.

2G). The excretion of the intracellular Cu may be attributed to exocytosis of PEG-HCuSNPs by both hepatocytes and Kupffer cells, which was supported by the *in vitro* transwell endo/exocytosis results showing fast excretion of PEG-HCuSNPs by both hepatocytes and Kupffer cells. These evidence taken together indicated that Kupffer cells might serve as a reservoir for storage of the blood-circulating PEG-HCuSNPs without significant metabolism.

Metabolic pathway of PEG-HCuSNPs in liver following i.v. injection. Based on the above results, we propose the itinerary of the metabolic process of PEG-HCuSNPs in liver following i.v. injection as shown in Scheme 1. As soon as PEG-HCuSNPs enter blood circulation, the nanoparticle's surface immediately adsorbs serum proteins and/or peptides forming a protein corona. The nanoparticles activate complement component C3 but not C5 in situ. The complements C3 and C3b play a key role in opsonization of PEG-HCuSNPs, facilitating their phagocytosis by Kupffer cells through interaction between C3/C3b and their respective receptors. However, Kupffer cells do not significantly metabolize the phagocytosed PEG-HCuSNPs but use it for temporary storage. The engulfed PEG-HCuSNPs may be excreted into blood circulation through exocytosis. On the other hand, the majority of PEG-HCuSNPs pass through the sieve plate of the sinusoid followed by endocytosis by hepatocytes. In contrast to Kupffer cells, hepatocytes quickly launch the endogenous detoxification mechanism in the presence of high intracellular loading of CuS nanoparticles. The nanoparticles either completely or partially break down into smaller CuS nanoparticles in endolysosomal compartments. Cu ions also dissociate in the endocytic vesicles during the nanoparticle's disintegration, further released into the cytosol. Cu-ATPase

ATP7B chelates the cytosolic Cu ions and redistributes from TGN to late endosome/lysosome compartments that fuse with the apical plasma membrane to excrete Cu ions into bile canaliculi. Moreover, ATP7B traverse the CuS nanoparticle-loaded vesicles participating in the removal of intra-vesicular Cu through chelating both particulate and ionic Cu. As a result, hepatocytes are the main force degrading PEG-HCuSNPs from blood circulation and excreting Cu in both particulate and ionic forms into bile. Kupffer cells in turn serve as a reservoir for transient storage of PEG-HCuSNPs in order to reduce the Cu surge in blood. Both cells play different roles in maintaining Cu homeostasis in the body.

Enhanced excretion of gold nanoparticles by HCuSNPs conjugation through ATP7B. We isolated primary hepatocytes from BALB/c mice by our modified two-step collagenase digestion method[19, 37, 38] with high purity (Fig. 3A). It is reported that functional bile canaliculi can be detected by fluorescence microscopy following 30 min incubation with 5 (6)-carboxy-2',7'-dichlorofluorescein diacetate (CDFDA), which can passively diffuses into hepatocytes, where it is hydrolyzed to fluorescent carboxy-dichlorofluorescein (CDF) only by functional polarized hepatocytes. After that, CDF is excreted into bile canaliculi.[49] After 48 h incubation of the seeded hepatocytes on collagen gel, much more CDF was formed and excreted into bile canaliculi compared to the cells only incubated for 24 h. (Fig. 6A) The ATP7B also correlative formed more after 48 h incubation compared to the 24 h incubation, and stayed around the nucleus. (Fig. 6B) The above data denoted that the perfused hepatocytes need 48 h to form ATP7B and for the polarized anatomy structure-bile canaliculi to function properly. After that, we treated cells with PEG-

HCuSNPs-RITC and CDFDA together and found that HCuSNPs colocalized with CDF, which can be excreted into bile canaliculi. It suggested HCuSNPs were excreted into bile canaliculi at last. Meanwhile, PEG-HCuSNPs-FITC was also colocalized with ATP7B (Fig. 6C and 6D), denoted that HCuSNPs were excreted into bile canaliculus facilitated by ATP7B.

With this finding, we then want to find out whether the excretion of HCuSNPs can be used to enhance the gold nanoparticles excretion. Gold nanosphere (~40nm) conjugated to the HCuSNPs (PEG-HCuSNPs@Au) (Fig. 7A) were used to treat primary cultured hepatocytes with CDFDA. After 30 min incubation, PEG-HCuSNPs@Au was colocalized with CDF and ATP7B, (Fig. 7B and 7C) however, in PEG-AuNP group, CDF was excreted into the bile canaliculi without the PEG-AuNP (Fig. 7B). Moreover, PEG-AuNPs after endocytosis were not colocalized with ATP7B in the cultured hepatocytes and still stayed in cells. (Fig. 7C) The quantitative analysis of gold exocytosis rate between PEG-AuNP and PEG- HCuSNPs@Au was also studied using transwells seeded with mouse and human primary hepatocyte to mimic the *in vivo* environment. In mouse primary hepatocytes, 36.10% of PEG-AuNPs were excreted out in the first 30 min and kept at around 15% after 60 min exocytosis process, however, 55.10% of PEG-HCuSNPs@Au were excreted in the first 30 min and keep at around 8% after 60 min exocytosis. (Fig. 8A and 8B) In human primary hepatocyte, 36.64% of PEG-AuNPs were excreted in the first 10 min and kept at around 35% after 60 min exocytosis. PEG-HCuSNPs@Au excreted 54.47% in the first 10 min and kept at around 17% after 60 min exocytosis. (Fig. 8C and 8D) It suggested from the mouse and human primary hepatocytes transwell studies that PEG-

HCuSNPs@Au had a much faster excretion rate than the PEG-AuNPs alone. Meanwhile, less gold was left after 60 min excretion in the PEG-HCuSNPs@Au treated group, which denoted that HCuSNPs not only increased the gold excretion rate, also enhanced the clearance of gold from the hepatocytes significantly and had less gold residue within cells. We looked further into the *in vivo* PEG-HCuSNPs@Au nanoparticles excretion. Bile samples collected from gall bladders at different times following intravenous (i.v.) injection of the PEG-HCuSNPs@Au nanoparticles in BALB/c mice. Transmission electron microscopy (TEM) illustrated that the nanoparticles appeared in bile as early as 15 min after the administration. Particles were also seen in 30 min, 1 h, and 4 h time points. (Fig. 9)

Besides the gold sphere, we also synthesized gold nanorod (AuNR) (~40nm) and AuNR conjugated with CuSNPs(~5nm) (PEG-AuNR@CuS) (Fig. 10A) to compare the excretion process between gold nanorod and PEG-AuNR@CuS. At 5 min after the CuSNPs treatment, PEG-CuSNPs already colocalized with ATP7B, which moved from cytosol to along with the bile canaliculi in a fast rate. The same observation happened in the PEG-AuNR@CuS treated group. (Fig. 10B and D) However, after 35 min treated with PEG-AuNR alone, the nanorods were still within the hepatocytes and not overlap with ATP7B. (Fig. 10C) After 35 min incubation with CDFDA, PEG-CuSNPs and AuNR@CuS were excreted into bile canaliculi together with CDF. However, PEG-AuNRs were still within hepatocytes. (Fig. 10E) It suggested that conjugating PEG-AuNR@CuS facilitated the excretion of PEG-AuNR into bile canaliculi. Meanwhile, the exocytosis rate of gold was compared between PEG-AuNR and PEG-AuNR@CuS using transwells seeded with primary cultured

mouse and human hepatocytes to mimic the *in vivo* environment. In mouse primary hepatocyte, in the PEG-AuNR treated group, 38.3% of gold were excreted out in the first 10 min and still 10% left after 60 min exocytosis, However, 87.7% of gold in the PEG-AuNR@CuS treated group were drained in first 10 min, and less than 1% left after 60 min exocytosis. (Fig. 11A and 11B) The fast excretion rate of PEG-AuNR@CuS also happens in human primary hepatocytes. In the PEG-AuNR treated group, 59.6% of gold were excreted out in the first 10 min and still 1.5% left after 60 min exocytosis, However, in the PEG-AuNR@CuS treat group, 80.5% of gold in the AuNR@CuS treated group were drained in first 10 min, and less than 0.7% left after 60min exocytosis. (Fig. 11C and 11D). Based on the transwell endo/exocytosis study, even though we synthesized gold and copper sulfide nanoparticles in different sizes and shapes, the exocytosis rate of gold will increase dramatically after conjugation of gold and copper sulfide nanoparticles compared to gold nanoparticles only.

CONCLUSION

In conclusion, we clearly elucidated the liver metabolic pathway of PEG-HCuSNPs in which hepatocytes played a major role in taking up, degrading and eliminating the nanoparticles through efficient hepatobiliary excretion. Cu-ATPase ATP7B were the key transporter participating in the removal of excess Cu in both particulate and ionic forms through trafficking toward the apical membrane of hepatocytes. In contrast, metabolism of PEG-HCuSNPs in Kupffer cells was minimal although their phagocytosis was significant through opsonization. The function of Kupffer cells was likely to reduce the copper surge in blood through storage of the nanoparticles, but with limited capacity. Additionally, apply the fast metabolism and clearance rate of CuSNPs, it was not only increased the gold excretion rate, also enhanced the clearance of gold from the hepatocytes significantly after conjugating the AuNPs with CuSNPs. Our findings will give deeper insight to understand the relationship between metabolism and toxicity of CuS nanoparticles in the hepatobiliary system and also the application of its advantage properties such as fast metabolism to enhance to clearance of other heavy metallic particles.

EXPERIMENTAL SECTION

Materials. Chemicals were ordered from Sigma-Aldrich Co. LLC. unless described specifically. The primary hepatocytes are cultured with Williams' Media E (WEM, Fisher Scientific) that was supplemented with 10% FBS and 1% penicillin-streptomycin. BALB/c mice were purchased from Jackson Laboratory, Inc. All animal experiments were performed under protocols approved by the University of Rhode Island and Fudan University Institutional Animal Care and Use Committee (IACUC).

Synthesis of HCuSNPs. The HCuSNPs were synthesized according to a previously reported method with minor modifications.[50] $CuCl_2$ solution (500μL, 0.5mol L^{-1}) was added to deionized water containing poly-(vinylpyrrolidone) (PVP-K30,) in a round flask under magnetic stirring at room temperature. Then, NaOH solution (25 mL, pH 9.0) was added to the mixture. After stirring for 5 min, hydrazine anhydrous solution was added to form a suspension of Cu_2O spheres. Another 5 min later, freshly prepared Na_2S aqueous stock solution (2.5 mL, 320 mg/mL) was added to the suspension. The flask was heated for 2 h at 60°C with magnetic stirring. After incubating overnight at room temperature, the HCuSNPs were centrifuged at 11,000 rpm for 15 min at room temperature, and washed twice with distilled water. HCuSNPs was resuspended in 4.8 mL of water mixed with 200 μL of Methoxy-PEG5$_K$-SH (20 mg/mL,) overnight at room temperature to obtain PEG-HCuSNPs. The nanoparticles were then washed twice with distilled water and stored at 4 °C for future use.

Synthesis of Au-nanorod (two-step method) Au-nanorod was synthesized according to a two-step method with modifications.[51, 52, 53] 1) Seed Synthesis The synthesis was performed in a 27°C water bath. After adding 25 μl of 50 mM $HAuCl_4$

solution to 4.7 ml of 0.1 M CTAB, the mixture was slowly stirred for 5 min. Then, 300 μL of a freshly prepared 10 mM $NaBH_4$ was rapidly injected under vigorous stirring. After 20 seconds, the solution (light brown color) is gently stirred and incubated for 30 min before use. 2) Synthesis of Au nanorod Ten ml of 0.01 M $HAuCl_4$ solution was added to 190 ml of 0.1 M CTAB. The mixture is gently shaken and incubated 10 min in a 27°C water bath to ensure uniformly mixed between gold salt and CTAB. Afterwards, ascorbic acid solution (1.1 mL, 0.1 M) is added to the mixture, which was gently shaken for few seconds until the solution turned colorless. A solution of $AgNO_3$ (1.6 mL, 0.01 M) was then added to the solution, which was shaken for few seconds. Finally, the seeds solution (240 μL) was added to the mixture and the solution was vigorously shaken and left undisturbed in a 27 °C water bath overnight. The OD of the solution was checked by wavelength scan and the peak was around 750 nm. The size was around 40 nm, as determined by TEM conformation.

Synthesis of Au-nanosphere Five grams of chlorauric acid in 95 mL of solution was heated to the boiling point with stirring and 5 mL of 10 mg/mL sodium citrate solution was added to the boiling solution. After about a minute of stirring, a very faint greyish-pink tone appeared, which gradually darkened over a period of about 10 min. The final color of the solution was deep wine red.[54]

Synthesis of AuNR@CuS conjugation In day one, 0.5 mg of Au rod (prepared according to above method) was mixed with 1 mg of SH-$PEG5_K$-Methoxy and 0.1 mg of SH-$PEG5_K$-COOH in 1 mL Millipore water. Then the mixture was sonicated for 10 min and left on the rotor plate for overnight at room temperature. On day two, a 50°C water bath was prepared before the synthesis process. In a 50 ml

falcon tube, added 9 ml of ddH_2O was added and stirred. The following reagents were sequentially: (100 μL, 100 mM) $CuCl_2$, (50 μL, 5 mg) SH-PEG5$_K$-M, (1 mL, 6.1 mg) GSH. The pH of the mixture was adjusted with NaOH to pH 9.3. Then the mixture was vented with argon for 5 min, followed by addition of thioacetamide. After that, the mixture was kept in a 50 °C water bath with magnetic stirring for 2 h, then the CuSNPs was condensed for 15 min, 4000 g in swing bucket, and then the condensed particle was resuspended in diH_2O.[55]

On day two, the PEG-AuNRs was activated with 0.4 mg (3-Dimethylaminopropyl)-N-ethylcarbodiimide hydrochloride (EDC-HCl) and 0.6 mg N-Hydroxysuccinimide (NHS) and placed on the rotor plate to activate for 1 h at room temperature. After activation, AuNRs were centrifuged for 10 min at 14,000 rpm and the supernatant was discarded. The AuNRs were washed in cold MES twice. Then the pellet was washed in 1 mL 1XPBS and centrifuged for 10 min at 14,000 rpm. One mL of AuNRs was added to 4 mL of CuSNPs. After 15 min sonication, the mixture was placed on the rotor plate for 24 h mixing at room temperature. On day three, the mixture was centrifuged at 11000 rpm for 10 min to remove the unconjugated CuSNPs. Then the pellet was washed for twice and stored in 100 μL of diH_2O at 4°C.

Synthesis of PEG-HCuSNP@Au conjugation. The PEG-HCuSNP@Au conjugation underwent a one-step synthesis according to a previous publication with modification.[56] One mL of HCuSNPs suspension as prepared above was dispersed in 1.2 mL ethanol, followed by the addition of 10 mg PVP-K30. After stirring for 30 min, 9.6 mL $HAuCl_4 \cdot 3H_2O$ aqueous solution (0.3 mM) was added and the mixture was stirred for 10 min. Afterward, 0.5 mL $NaBH_4$ (3 mM) was added and the mixture

was stirred for another 30 min. The products were collected by centrifugation at 11000 rpm for 15 min and washed three times with ethanol. Then, the PEG-HCuSNP@Au conjugations were resuspended in water and coated with SH-PEG5$_K$-Methoxy.

Excretion of PEG-HCuSNPs into gall bladders in mice. BALB/c mice were divided into 7 groups (n = 3 - 4). One group of mice injected with saline were used as blank control. The other 6 groups received i.v. injection of PEG-HCuSNPs (20 mg/kg body weight of Cu). At 1 h, 4 h, 24 h, 2 d, 4 d, or 7 d post-injection, the gallbladder of each mouse was collected. The content of each gallbladder was then centrifuged at 13,523 g for 15 min to separate the pellet (CuS nanoparticles) and supernatant (Cu ions). The supernatant of each sample was directly added to a 2% nitric acid solution for inductively coupled plasma mass spectrometer (ICP-MS) analysis (Model: X7, Thermo Electron Corporation) of Cu. The pellet was added with nitric acid and digested by Mars 5 microwave system (CEM Corporation), 0.2 mL of which was added to 9.8 mL of deionized water for ICP-MS analysis. In a parallel study, the pellet was resuspended in water and directly deposited on the Formvar-coated nickel grid (200 mesh, Ted Pella, Inc.) without counterstaining. The samples were examined under TEM (JEOL, JEM2100).

Isolation of Primary Mouse Hepatocytes and Kupffer Cells. Primary mouse hepatocytes and Kupffer Cells were isolated by a two-step collagenase perfusion. After perfusion mouse liver was excised and finely broken into small pieces by forceps in washing buffer. The resulting cell suspension was passed through a 40-mm cell strainer to remove undigested tissue. The resulting single-cell suspension was obtained and transferred to a 50 ml conical tube and centrifuged at 50 g for 5 min at 4

°C. The supernatant was saved for the non-parenchymal cells (NPC) including (Kupffer Cells) purification. The hepatocyte pellet was further purified with 100% Percoll (GE). After washing, the high-purified hepatocytes were resuspended in culture medium for future use.[57] The NPC (including Kupffer cells) was centrifuged at 650 g for 7 min at 4 °C. The collected pellets (NPC) were purified with 50% Percoll to remove blood cells. For Kupffer Cells purification: 10 μL PE-conjugated anti-F4/80 antibody was added in the dark for 15 min at 4 °C, then washed with 1mL BPE (phosphate-buffered saline (PBS), pH 7.2, 0.5% bovine serum albumin (BSA), and 2 mM EDTA) and centrifuged at 650 g for 7 min at 4 °C. The pellet was resuspended in 100 μL BPE and 20 μL anti-PE beads and incubated in the dark for 15 min at 4 °C. It was then washed with 1 mL BPE, and centrifuged again at 650 g for 7 min at 4°C. The supernatant was removed and the pellet was resuspended in 500 μL BPE. After that, the column was placed in the magnetic field of the MACS separator. After rinsing the column with 500 μL BPE, 500 μL cell suspension was applied to the column. Kupffer Cells were collected after the unlabeled cells were washed out.[58]

Proteomics analysis of PEG-HCuSNPs-bound proteins. Two groups of BALB/c mice were i.v. injected with PEG-HCuSNPs (20 mg/kg of Cu). After 5 or 60 min, the mouse blood was collected in Eppendorf tubes containing 109 mM of sodium citrate (100 μL) as an anticoagulant, and centrifuged at 845 g for 5 min to obtain the mouse plasma, followed by a second centrifugation at 1,503 g for 3 min to further remove red blood cells. A third centrifugation at 1,503 g for 6 min resulted in a CuS pellet. The CuS pellet was washed with PBS once, then with 20 mM Tris-MOPS buffer (pH 7.4) for 6 times. Afterward, 50 μL of reducing buffer (62.5 mM Tris-

hydrochloride, 20 mM dithiothreitol, 2% sodium dodecyl sulfate, 20 mM EDTA, pH 6.8) was added to disperse the washed CuS pellet. The dispersion was heated at 70 °C for 10 min to detach the absorbed proteins from the nanoparticles. A centrifugation at 12,851 g for 10 min was performed to collect the supernatant for proteomic analysis.

Preparation of nanoparticle-bound proteins for Western blotting analysis. One hundred microliters of freshly collected mouse serum were added to 500 μL of PBS. Then, 400 μL of PEG-HCuSNPs (1 mg/mL of Cu) or PEG-HAuNS (1 mg/mL of Au) were added to the above PBS and incubated for 1 h at 37 °C on the rocker. After incubation, the samples were centrifuged at 12,851 g for 10 min to separate the pellet and supernatant. The supernatant was directly used for Western blotting analysis. After washed with 20 mM Tris-MOPS buffer (pH 7.4) for 6 times, the pellet was dispersed in 50 μL of reducing buffer (62.5 mM Tris-hydrochloride, 20 mM dithiothreitol, 2% sodium dodecyl sulfate, 20 mM EDTA, pH 6.8) and heated at 70 °C for 10 min to detach the absorbed proteins. A centrifugation at 12,851 g for 10 min was performed to collect the nanoparticle-bound proteins in the supernatant for proteomic analysis.

CDFDA Assay. The mouse primary hepatocytes were cultured for 48 h in a collagen-coated petri dish. The hepatocyte and bile canaliculi function was assessed by visualization of excreted fluorescent products after incubation with 5-(and-6)-carboxy-2′,7′- dichlorofluorescein diacetate (carboxy-DCFDA) at a final concentration of 2 μM. Carboxy-DCFDA molecule can passively enter the cytoplasm of functional hepatocytes, where esterase metabolizes it to a fluorescent product that is then

excreted into the bile canaliculi only by functional hepatocytes. The cell nuclei were counterstained using Hoechst 33342.[59]

Confocal Study of Nanoparticles Excretion Process. Mouse primary hepatocytes were cultured in collagen coated 35-mm petri dish. After 48 h incubation, cells were treated with 10 μg/mL of different kinds of nanoparticle-FITC for 5 min, 15 min and 35 min. The cells were stained with rabbit anti mice antibody ATP7B (Santa Cruz) and counterstained with goat anti rabbit- Alexa fluor-555 (Invitrogen). The cell nuclei were counterstained using DAPI (Sigma). Confocal fluorescence images were obtained with a Zeiss axioimager M2 imaging system with Zeiss LSM 700 confocal module.

Primary cultured hepatocytes and Kupffer cells on Transwell for Endo/Exocytosis Study 1) Endocytosis: Transwells were coated with 50 μg/ml type I collagen in 0.02 N glacial acetic acid. The transwells were incubated for one hour at room temperature and then washed with a 4 fold volume of 1X PBS. Then transwells were coated with 1.5 mg/mL collagen and incubated in the cell culture incubator for 15 min. A single layer of hepatocytes was seeded two days before the experiment. In the upper chamber, 500 μL cell culture media was added and 1500 μL of cell culture media was added to the lower chamber. Nanoparticles (10 μg/mL) were incubated with WME with 2% mouse serum final concentration for one hour. The apical side media was aspirated and replaced with 500 μL of nanoparticles included media and incubated for 5 min at 37 ^{o}C. The apical medium was removed and washed twice with ice-cold PBS to stop the endocytosis process. After washing the insert, 100 μL of CelLytic M cell lysis reagent was added to the apical side of the transwells. The cell

lysate was collected and transferred into a 1.5 mL Eppendorf tubes. Then, the lysate was centrifuged at 13,523 g for 10 min and the supernatant was removed from the pellet and stored at 4 ^{o}C separately. 2) Exocytosis: Endocytosis is the same process as described above. After 5 min incubation at 37 ^{o}C, media with nanoparticles in the upper chamber side was aspirated and quickly washed with 500 uL warm WME once, and then 500 μL of fresh cell culture media was added into the upper chamber side. The cell culture insert was transferred to another well with 1.5 mL of cell culture media. After 10 min, the upper chamber media was aspirated and washed with 500 μL of warm WME on both sides. Then 100 μL CelLytic M cell lysis reagent was added to the upper chamber and cell lysate was transferred into a 1.5 mL Eppendorf tubes. After another 30 min and 1 h, the above exocytosis step was repeated. The collected cell lysates were centrifuged at 13,523 g for 10 min, and the pellet was moved from the supernatant for the ICP-MS analysis.

ICP-MS Analysis The endo/exocytosis samples were dissolved in 4 parts HNO_3 and 1 part HCl overnight for digestion. Before loading the sample to the inductively coupled plasma mass spectrometer (ICP-MS) (Model: X7, Thermo Electron Corporation) for quantitative analysis of Cu or Au, the solvent was diluted to 2% HNO_3 / 2% HCl. The calibration standards of Cu and Au have six concentrations (0.1, 0.25, 1, 25, 50, 100, and 200 ppb) and were analyzed with each batch of samples.[19]

Preparation of tissue samples for TEM. BALB/c mice were i.v. injected with PEG-HCuSNPs (20 mg/kg of Cu). At the predetermined time points, the mice were euthanized and the liver was quickly collected, cut into 1 mm^3 and fixed in the

fixation reagent (2.5% glutaraldehyde plus 2% paraformaldehyde in 0.1 M phosphate buffer, pH 7.4). The TEM sample preparation followed routine procedure. The samples were embedded in Epon resin followed by ultrathin sectioning (60-70 nm thickness). The sections were placed on nickel grids with formvar/carbon film stained with 7% uranyl acetate and lead citrate. The samples were examined under TEM microscope (FEI Tecnai Biotwin, LaB6, 80 kV).

Immunofluorescence staining. BALB/c mice were i.v. injected with PEG-HCuSNPs-FITC (20 mg/kg of Cu). At the predetermined time points, the mice were euthanized and the liver was quickly collected, and embedded in O.C.T. for cryosectioning (8 μm thickness). Tissue sections on slides were fixed in 95% methanol or acetone (10 min, -20°C), rehydrated in PBS, blocked in 2% BSA-PBS-0.15% Triton X100 (30 min), labeled with primary antibody (overnight, 4°C) and then secondary antibody (1 h, room temperature). Goat anit-ATP7B primary antibody from Santa Cruz Biotechnologies was diluted into 1:50 before use. Rabbit anti-Rab7 primary antibody from Abcam was diluted into 1:300 before use. CFL405 conjugated donkey anti-rabbit IgG (1:100) and CFL555 conjugated donkey anti-goat IgG (1:200) secondary antibodies were purchased from Santa Cruz Biotechnologies. The immunofluorescence-stained sections were examined under a ZEISS LSM 710 confocal microscope equipped with a 63x1.4 numerical aperture oil objective and ZEISS ZEN 2012 software.

Preparation of membrane and cytosol fractions of hepatocytes. Membrane and cytoplasmic fractions from the perfused primary hepatocytes in mouse at different times following injection of PEG-HCuSNPs (20 mg/kg of Cu) were prepared as

previously described with some modification. Approximately 100 mg of mouse primary hepatocytes were lysed and homogenized in 900 μL of sucrose-Tris (pH 7.2) buffer containing 250 mM of sucrose, 1 mM of EDTA, 10 mM of Tris HCl, and protease inhibitors (100x Halt Protease and Phosphatase Inhibitor Cocktail, ThermoFisher). The homogenates were sonicated for three times (10 s per pulse, 30 s interval). The lysates received first centrifugation at 500 g for 10 min to remove cellular debris. A second centrifugation at 6,000 g for 10 min was used to pellet the CuS nanoparticles. A third centrifugation at 100,000 g for 60 min was applied to separate cytosolic fractions from the lysates. The pellets were then washed with 900 μL of sucrose-Tris buffer and centrifuged at 100,000 g for 60 min. After washing, the pellets were suspended with 50 μL sequential extraction kit reagent 3 (Bio-Rad), and centrifuged at 100,000 g for another 60 min. The resulting supernatant was membrane fractions. All experiment was conducted at 4°C. The total protein concentration of these samples is determined using Pierce 660 nm Protein Assay Reagents (ThermoFisher).

Western blotting analysis. Western blotting was used to identify and semi-quantify proteins of interest isolated from the above samples. Thirty micrograms of total protein premixed with Laemmli buffer (Bio-Rad) containing 0.1% β-mercaptoethanol was loaded per well for sodium dodecyl sulfate-polyacrylamide gel electrophoresis (SDS-PAGE, Bio-Rad 4-20% Mini-PROTEAN TGX Precast Protein Gel). The proteins were transblotted on Bio-Rad PVDF membrane at 120 V for ~ 70 min. After the transfer, the membrane was blocked for 2 h in 1x Tris-buffered saline with 0.1% of Tween 20 (TBST) and 8% nonfat dry milk at room temperature. The

membrane was then incubated with mouse anti-ATP7B monoclonal antibody (1:500, Santa Cruz) or mouse anti-β-Actin monoclonal antibody (1:5,000, Sigma) in TBST overnight at 4°C. After TBST-washing, the membrane was incubated with goat anti-mouse HRP secondary antibody (1:10,000, Novex) for 1 hour at room temperature. The membrane was then washed and incubated with an ECL fluorescence kit (Bio-Rad Clarity™ Western ECL Substrate) or SuperSignal West Femto Maximum Sensitivity Substrate (Thermo scientific). Membranes were exposed in Gel Logic 2200 Pro and were qualified with ImageQuant TL Image Analysis Software (GE Healthcare). Levels of β-Actin were used to normalize ATP7B expression in cytosol and membrane. For Western blotting analysis of the nanoparticle-bound complement C3 and C5, rat anti-mouse Complement C3 monoclonal antibody (1:200, Santa Cruz), rat anti-mouse Complement C5a monoclonal antibody (1:200, MyBioSource), and goat anti-rat HRP secondary antibody (1:10,000, Santa Cruz) were used.

Quantitative real-time PCR for Atp7b mRNA analysis in mouse hepatocytes. Total RNA from the perfused primary hepatocytes in mouse at different times following injection of PEG-HCuSNPs (20 mg/kg of Cu) was isolated using RNA-Bee reagent (AMS Biotechnology) according to the manufacturer's protocol. The RNA was quantified by measuring its absorbance at 280 nm with a UV-visible spectrophotometer (NanoDrop ND 1000, ThermoFisher). All the samples were diluted to 500 ng/μL concentration. The first-strand cDNA was synthesized using GoScript Reverse Transcription System (Promega). The cDNAs were diluted six times with water and subjected to real-time PCR using TaqMan Gene Expression Assay, following the instructions of the manufacturer. The TaqMan assay mixture for mouse

ATP7B (assay ID: Mm00599675_m1) and glyceraldehyde-3-phosphate dehydrogenase (GAPDH, assay ID: Mm99999915_g1) were purchased from ThermoFisher. Transcript levels of ATP7B were normalized against to GAPDH levels. Amplification and quantification were done with a ViiA7 Real-Time PCR System (Applied Biosystems).

Conflict of Interest: The authors declare no competing financial interest.

Supporting Information Available: Characterization and dissociation of PEG-HCuSNPs, release of FITC from the FITC-conjugated HCuSNPs and Western blotting analysis of ATP7B.

Acknowledgment. The authors thank Richard Kingsley from the University of Rhode Island for assisting in TEM of nanoparticles, Carol Ayala from Rhode Island Hospital and Xinran Liu from Yale University for assisting in preparation and TEM of liver tissue samples, and James Clifton from Brown University for assisting in proteomic analysis. This work was partially supported by the 973 project of China (2013CB932500), the award of the "National Youth Thousand Talents Plan" of China, the Program for Professor of Special Appointment (Eastern Scholar) at Shanghai Institutions of Higher Learning (No.2012-05), and by grants from the National Institute of Health (R01EB018748, P20GM103430 and P20GM104937).

References

1. Li, Y.; Lu, W.; Huang, Q.; Huang, M.; Li, C.; Chen, W., Copper sulfide nanoparticles for photothermal ablation of tumor cells. Nanomedicine (Lond) 2010, 5, 1161-71.

2. Tian, Q.; Jiang, F.; Zou, R.; Liu, Q.; Chen, Z.; Zhu, M.; Yang, S.; Wang, J.; Wang, J.; Hu, J., Hydrophilic Cu9S5 nanocrystals: a photothermal agent with a 25.7% heat conversion efficiency for photothermal ablation of cancer cells in vivo. ACS Nano 2011, 5, 9761-71.

3. Tian, Q.; Tang, M.; Sun, Y.; Zou, R.; Chen, Z.; Zhu, M.; Yang, S.; Wang, J.; Wang, J.; Hu, J., Hydrophilic flower-like CuS superstructures as an efficient 980 nm laser-driven photothermal agent for ablation of cancer cells. Adv Mater 2011, 23, 3542-7.

4. Xiao, Z., CuS nanoparticles: clinically favorable materials for photothermal applications? Nanomedicine. 2014, 9, 373-5.

5. Ramadan, S.; Guo, L.; Li, Y.; Yan, B.; Lu, W., Hollow copper sulfide nanoparticle-mediated transdermal drug delivery. Small 2012, 8, 3143-50.

6. Guo, L.; Yan, D. D.; Yang, D.; Li, Y.; Wang, X.; Zalewski, O.; Yan, B.; Lu, W., Combinatorial photothermal and immuno cancer therapy using chitosan-coated hollow copper sulfide nanoparticles. ACS Nano 2014, 8, 5670-81.

7. Dong, K.; Liu, Z.; Li, Z.; Ren, J.; Qu, X., Hydrophobic anticancer drug delivery by a 980 nm laser-driven photothermal vehicle for efficient synergistic therapy of cancer cells in vivo. Adv Mater 2013, 25, 4452-8.

8. Ku, G.; Zhou, M.; Song, S.; Huang, Q.; Hazle, J.; Li, C., Copper sulfide nanoparticles as a new class of photoacoustic contrast agent for deep tissue imaging at 1064 nm. ACS Nano 2012, 6, 7489-96.

9. Wang, Z.; Huang, P.; Jacobson, O.; Wang, Z.; Liu, Y.; Lin, L.; Lin, J.; Lu, N.; Zhang, H.; Tian, R., et al., Biomineralization-Inspired Synthesis of Copper Sulfide-Ferritin Nanocages as Cancer Theranostics. ACS Nano 2016, 10, 3453-60.

10. Zhou, M.; Zhang, R.; Huang, M.; Lu, W.; Song, S.; Melancon, M. P.; Tian, M.; Liang, D.; Li, C., A chelator-free multifunctional [64Cu]CuS nanoparticle platform for simultaneous micro-PET/CT imaging and photothermal ablation therapy. J Am Chem Soc 2010, 132, 15351-8.

11. Zhou, M.; Li, J.; Liang, S.; Sood, A. K.; Liang, D.; Li, C., CuS Nanodots with Ultrahigh Efficient Renal Clearance for Positron Emission Tomography Imaging and Image-Guided Photothermal Therapy. ACS Nano, 2015, 9, 7085-96.

12. Chen, F.; Hong, H.; Goel, S.; Graves, S. A.; Orbay, H.; Ehlerding, E. B.; Shi, S.; Theuer, C. P.; Nickles, R. J.; Cai, W., In Vivo Tumor Vasculature Targeting of CuS@MSN Based Theranostic Nanomedicine. ACS Nano 2015, 9, 3926-34.

13. Xiao, Q.; Zheng, X.; Bu, W.; Ge, W.; Zhang, S.; Chen, F.; Xing, H.; Ren, Q.; Fan, W.; Zhao, K., et al., A core/satellite multifunctional nanotheranostic for in vivo imaging and tumor eradication by radiation/photothermal synergistic therapy. J Am Chem Soc 2013, 135, 13041-8.

14. Zha, Z.; Zhang, S.; Deng, Z.; Li, Y.; Li, C.; Dai, Z., Enzyme-responsive copper sulphide nanoparticles for combined photoacoustic imaging, tumor-selective chemotherapy and photothermal therapy. Chem Commun (Camb) 2013, 49, 3455-7.

15. Zhou, M.; Chen, Y.; Adachi, M.; Wen, X.; Erwin, B.; Mawlawi, O.; Lai, S. Y.; Li, C., Single agent nanoparticle for radiotherapy and radio-photothermal therapy in anaplastic thyroid cancer. Biomaterials 2015, 57, 41-9.

16. Zha, Z.; Wang, S.; Zhang, S.; Qu, E.; Ke, H.; Wang, J.; Dai, Z., Targeted delivery of CuS nanoparticles through ultrasound image-guided microbubble destruction for efficient photothermal therapy. Nanoscale 2013, 5, 3216-9.

17. Scheiber, I.; Dringen, R.; Mercer, J. F., Copper: effects of deficiency and overload. Met Ions Life Sci 2013, 13, 359-87.

18. Wang, Z.; von dem Bussche, A.; Kabadi, P. K.; Kane, A. B.; Hurt, R. H., Biological and environmental transformations of copper-based nanomaterials. ACS Nano 2013, 7, 8715-27.

19. Guo, L.; Panderi, I.; Yan, D. D.; Szulak, K.; Li, Y.; Chen, Y. T.; Ma, H.; Niesen, D. B.; Seeram, N.; Ahmed, A., et al., A comparative study of hollow copper sulfide nanoparticles and hollow gold nanospheres on degradability and toxicity. ACS Nano 2013, 7, 8780-93.

20. Pilot Study of Aurolase(Tm) Therapy in Refractory and/or Recurrent Tumors of the Head and Neck. http://clinicaltrials.gov/show/NCT00848042

21. Efficacy Study of Aurolase Therapy in Subjects with Primary and/or Metastatic Lung Tumors. http://clinicaltrials.gov/show/NCT01679470

22. Sharifi, S., Behzadi, S., Laurent, S., Forrest, M. L., Stroeve, P., & Mahmoudi, M. (2012). Toxicity of nanomaterials. Chemical Society Reviews, 41(6), 2323–2343. http://doi.org/10.1039/c1cs15188f 23. Chem Soc Rev. 2012; 41:2323–2343. [PubMed: 22170510]

24. Sadauskas, E., Danscher, G., Stoltenberg, M., Vogel, U., Larsen, A., Wallin, H. Protracted Elimination of Gold Nanoparticles from Mouse Liver. Nanomedicine. 2009; 5:162–169.

25. Balasubramanian, S., Jittiwat, J., Manikandan, J., Ong, C., Yu, L., Ong, W. Biodistribution of Gold Nanoparticles and Gene Expression Changes in the Liver and Spleen after Intravenous Administration in Rats. Biomaterials. 2010; 31:2034–2042.

26. Nirmala, G., Akila, S., Nadar, M., Narendhirakannan, R., Chatterjeeb, S. Biosynthesized Vitis vinifera seed gold nanoparticles Induce apoptotic cell death in A431 skin cancer cells, RSC Adv. 6 (2016) 82205-82218.

27. Cho, W.; Cho, M.;Jeong, J.; et al., Acute toxicity and pharmacokinetics of 13 nm-sized PEG-coated gold nanoparticles, Toxicol. Appl. Pharmacol. 236 (2009) 16-24.

28. De Jaeghere, F.; Allemann, E.; Leroux, J. C.; Stevels, W.; Feijen, J.; Doelker, E.; Gurny, R., Formulation and lyoprotection of poly(lactic acid-co-ethylene oxide) nanoparticles: influence on physical stability and in vitro cell uptake. Pharm Res 1999, 16, 859-66.

29. Doğan, A.; Köseoğlu, F.; Kılıç, E., The Stability Constants of Copper (II) Complexes with Some α-Amino Acids in Dioxan–Water Mixtures. Analytical biochemistry 2001, 295, 237-239.

30. Rigo, A.; Corazza, A.; di Paolo, M. L.; Rossetto, M.; Ugolini, R.; Scarpa, M., Interaction of copper with cysteine: stability of cuprous complexes and catalytic role of cupric ions in anaerobic thiol oxidation. Journal of inorganic biochemistry 2004, 98, 1495-1501.

31. Luza, S. C.; Speisky, H. C., Liver copper storage and transport during development: implications for cytotoxicity. The American journal of clinical nutrition 1996, 63, 812S-820S.

32. Wang, Z.; Von Dem Bussche, A.; Kabadi, P. K.; Kane, A. B.; Hurt, R. H., Biological and environmental transformations of copper-based nanomaterials. ACS nano 2013, 7, 8715-8727.

33. Polishchuk, E. V.; Concilli, M.; Iacobacci, S.; Chesi, G.; Pastore, N.; Piccolo, P.; Paladino, S.; Baldantoni, D.; van, I. S. C.; Chan, J., et al., Wilson disease protein ATP7B utilizes lysosomal exocytosis to maintain copper homeostasis. Dev Cell 2014, 29, 686-700.

34. Hasan, N. M.; Gupta, A.; Polishchuk, E.; Yu, C. H.; Polishchuk, R.; Dmitriev, O. Y.; Lutsenko, S., Molecular events initiating exit of a copper-transporting ATPase ATP7B from the trans-Golgi network. J Biol Chem 2012, 287, 36041-50.

35. Nyasae, L. K.; Schell, M. J.; Hubbard, A. L., Copper directs ATP7B to the apical domain of hepatic cells via basolateral endosomes. Traffic 2014, 15, 1344-65.

36. Bucci, C.; Thomsen, P.; Nicoziani, P.; McCarthy, J.; van Deurs, B., Rab7: a key to lysosome biogenesis. Mol Biol Cell 2000, 11, 467-80.

37. Shi, D.; Yang, D.; Yan, B., Dexamethasone transcriptionally increases the expression of the pregnane X receptor and synergistically enhances pyrethroid esfenvalerate in the induction of cytochrome P450 3A23. Biochem Pharmacol 2010, 80, 1274-83.

38. Yang, D.; Yang, J.; Shi, D.; Xiao, D.; Chen, Y. T.; Black, C.; Deng, R.; Yan, B., Hypolipidemic agent Z-guggulsterone: metabolism interplays with induction of carboxylesterase and bile salt export pump. J Lipid Res 2012, 53, 529-39.

39. Lorinczi, E.; Tsivkovskii, R.; Haase, W.; Bamberg, E.; Lutsenko, S.; Friedrich, T., Delivery of the Cu-transporting ATPase ATP7B to the plasma membrane in Xenopus oocytes. Biochim Biophys Acta 2008, 1778, 896-906.

40. Cuillel, M.; Chevallet, M.; Charbonnier, P.; Fauquant, C.; Pignot-Paintrand, I.; Arnaud, J.; Cassio, D.; Michaud-Soret, I.; Mintz, E., Interference of CuO nanoparticles with metal homeostasis in hepatocytes under sub-toxic conditions. Nanoscale 2014, 6, 1707-15.

41. Walkey, C. D.; Chan, W. C., Understanding and controlling the interaction of nanomaterials with proteins in a physiological environment. Chemical Society Reviews 2012, 41, 2780-2799.

42. Chonn, A.; Semple, S.; Cullis, P., Association of blood proteins with large unilamellar liposomes in vivo. Relation to circulation lifetimes. Journal of Biological Chemistry 1992, 267, 18759-18765.

43. Owens, D. E.; Peppas, N. A., Opsonization, biodistribution, and pharmacokinetics of polymeric nanoparticles. International journal of pharmaceutics 2006, 307, 93-102.

44. Vonarbourg, A.; Passirani, C.; Saulnier, P.; Simard, P.; Leroux, J.; Benoit, J., Evaluation of pegylated lipid nanocapsules versus complement system activation and macrophage uptake. Journal of biomedical materials research Part A 2006, 78, 620-628.

45. Karmali, P. P.; Simberg, D., Interactions of nanoparticles with plasma proteins: implication on clearance and toxicity of drug delivery systems. Expert opinion on drug delivery 2011, 8, 343-357.

46. Qin, X.; Gao, B., The complement system in liver diseases. Cell Mol Immunol 2006, 3, 333-340.

47. You, J.; Zhou, J.; Zhou, M.; Liu, Y.; Robertson, J. D.; Liang, D.; Van Pelt, C.; Li, C., Pharmacokinetics, clearance, and biosafety of polyethylene glycol-coated hollow gold nanospheres. Part Fibre Toxicol 2014, 11, 26.

48. Kumar, V., Target-oriented drug delivery systems. In Modern Pharmaceutics, Florence, A. T.; Siepmann, J., Eds. Informa Healthcare: New York, 2009; Vol. 2, pp 329-398.

49 Saab, L., Peluso, J., Muller, C., Ubeaud-Sequier, G. Implication of hepatic transporters (MDR1 and MRP2) in inflammation-associated idiosyncratic drug-induced hepatotoxicity investigated by microvolume cytometry, Cytometry Part A, vol. 83, no. 4, pp. 403–408, 2013.

50. Ramadan, S.; Guo, L.; Li, Y.; Yan, B.; Lu, W. Hollow Copper Sulfide Nanoparticle-Mediated Transdermal Drug Delivery. Small 2012, 8, 3143–3150.

51. Nikoobakht, B.; El-Sayed, M.A., Preparation and Growth Mechanism of Gold Nanorods (NRs) Using Seed-Mediated Growth Method. Chem. Mater. 2003, 15, 1957-1962.

52. Gou L.; Murphy, C., Fine-Tuning the Shape of Gold Nanorods. Chem. Mater. 2005, 17, 3668-3672.

53. Huang, X.; Neretina, S.; El-Sayed, M. A., Gold Nanorods: From Synthesis and Properties to Biological and Biomedical Applications. Adv. Mater. 2009, 21, 4880−4910.

54. Turkevich, J.; Stevenson, P; Hillier, J., A study of the nucleation and growth processes in the synthesis of colloidal gold. Discuss. Faraday Soc., 1951,11, 55-75. DOI:10.1039/DF9511100055

55. Liang, G.; Jin, X.; Qin, H.; Xing, D., Glutathione-capped, renal-clearable CuS nanodots for photoacoustic imaging and photothermal therapy. J. Mater. Chem. B, 2017, 5, 6366—6375.

56. Deng, X.; Kai, L.; Cai, X.; et al. A Hollow-Structured CuS@Cu2S@Au Nanohybrid: Synergistically Enhanced Photothermal Efficiency and Photoswitchable Targeting Effect for Cancer Theranostics[J]. Advanced Materials, 2017.

57. Kegel, V., Deharde, D., Pfeiffer, E., Zeilinger, K., Seehofer, D., Damm, G. Protocol for Isolation of Primary Human Hepatocytes and Corresponding Major Populations of Non-parenchymal Liver Cells. J. Vis. Exp. (109), e53069, doi:10.3791/53069 (2016).

58. Liu, W.; Hou, Y.; Chen, H.; Wei, H.; Lin, W.; Li, J.; Zhang, M.; He, F.; Jiang, Y., Sample preparation method for isolation of single-cell types from mouse liver for proteomic studies. Proteomics, 11: 3556–3564. doi:10.1002/pmic.201100157.

59. Tuschl, G.; Hrach, J.; Walter, Y.; Hewitt, PG.; Mueller, S.O., Serum-free collagen sandwich cultures of adult rat hepatocytes maintain liver-like properties long term: A valuable model for in vitro toxicity and drug–drug interaction studies. Chem Biol Interact. 2009; 181:124–137.

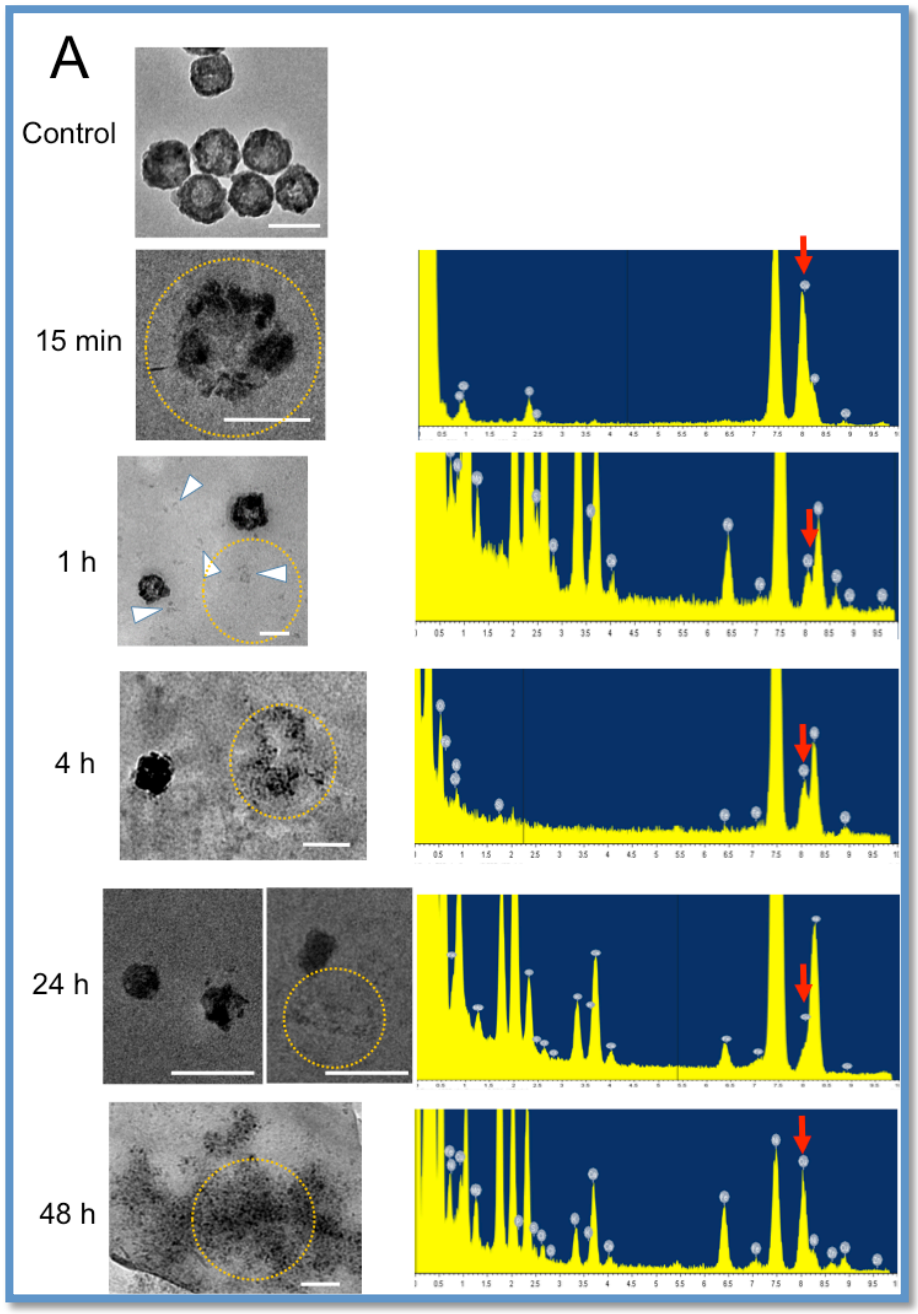
A
Control
15 min
1 h
4 h
24 h
48 h

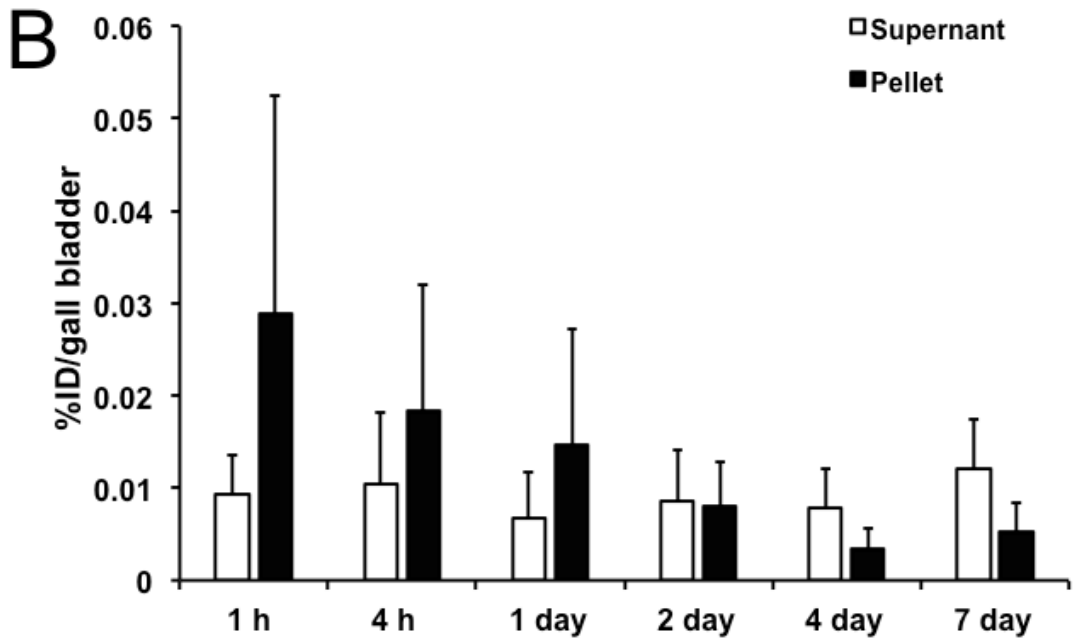

Figure 1. TEM of bile samples collected from BALB/c mice at different times following i.v. injection of PEG-HCuSNPs. (A), represent undisintegrated PEG-HCuSNPs without injection (Control). Or partially disintegrated large particles after 15min, 1h, 4h, 24h and 48h injection (B) The Cu levels in the supernatant (Cu ions) or pellet (CuS nanoparticles) of mouse gall bladder. The gall bladders were collected from BALB/c mice at different times after i.v. injection of PEG-HCuSNPs (20 mg/kg of Cu). Data are presented as mean ± standard deviation (n = 3 - 4).

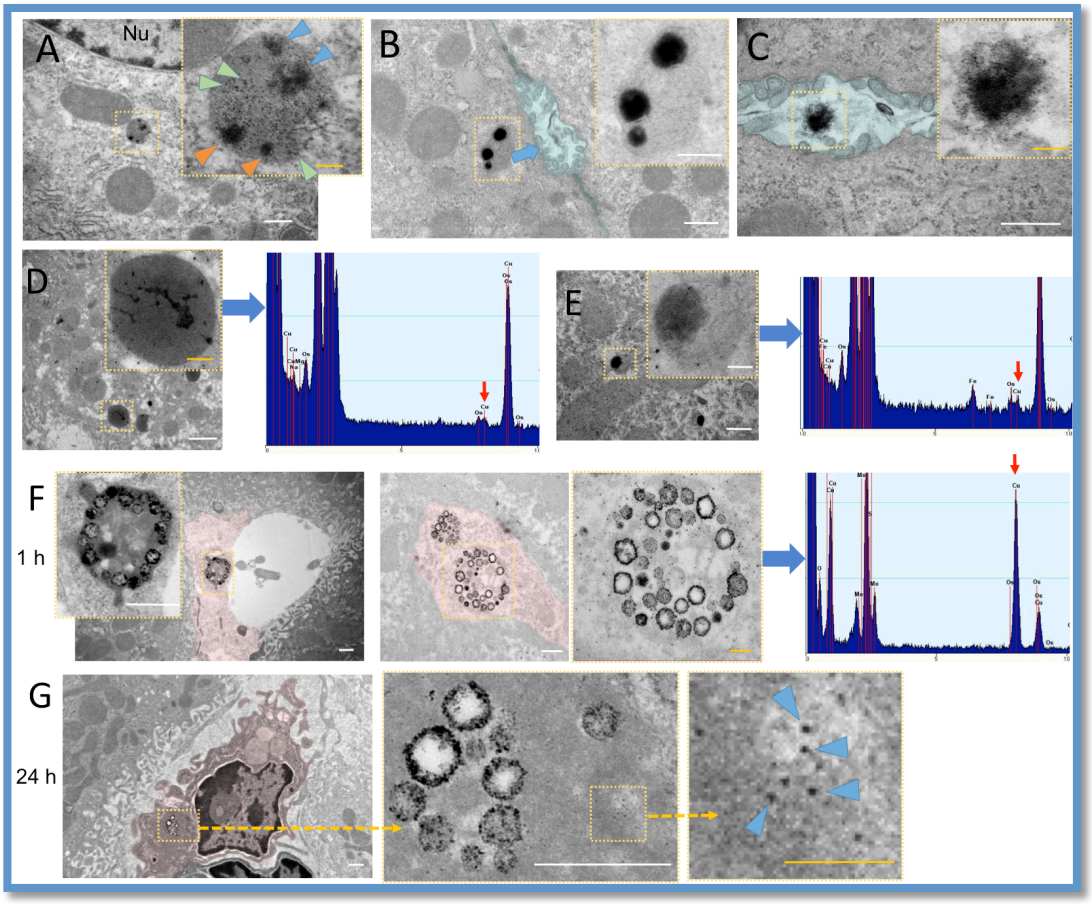

Figure 2. TEM of hepatocytes (A-E) in liver tissues of BALB/c mice at different times following i.v. injection of PEG-HCuSNPs. Blue arrowheads, partially disintegrated HCuSNPs; orange arrowheads, large particles with solid structures; green arrowheads, decomposed small CuS nanoparticles. Structures pseudo-colored in light cyan, bile canaliculi. Blue arrows, nanoparticle-loaded lysosomes moving toward bile canaliculi. Nu, nucleus. TEM of Kupffer cells (F-G) in liver tissues of BALB/c mice at different times following i.v. injection of PEG-HCuSNPs. Structures pseudo-colored in pink, Kupffer cells. Blue arrowheads, decomposed small CuS nanoparticles. Bars in white, 500 nm; bars in yellow, 100 nm.

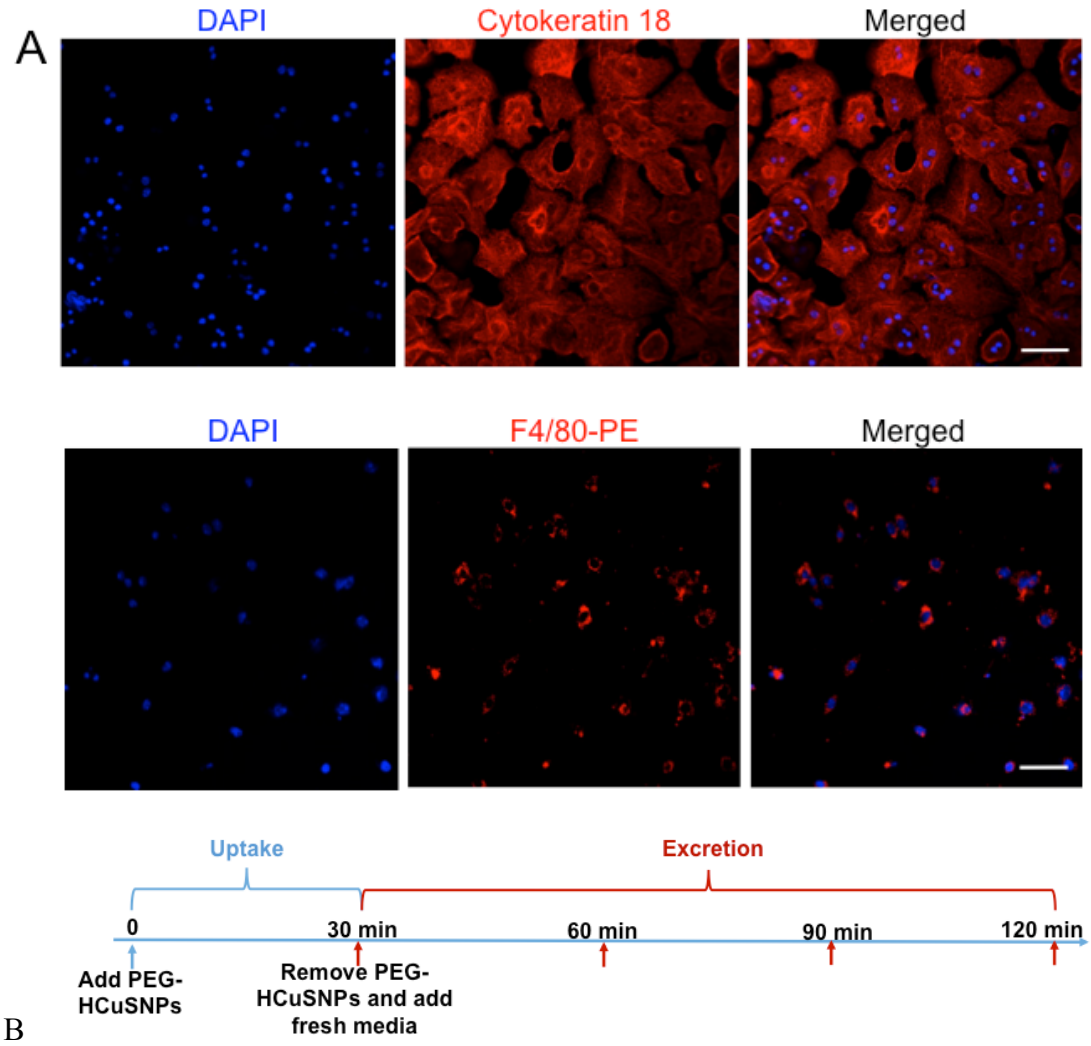
A
DAPI
Cytokeratin 18
Merged
DAPI
F4/80-PE
Merged
B
Uptake
Excretion
0
30 min
60 min
90 min
120 min
Add PEG-HCuSNPs
Remove PEG-HCuSNPs and add fresh media
Transwell
Nanoparticles
Upper chamber
Seeded Cell
Matrigel
Porous membrane
Cell culture medium
Lower chamber

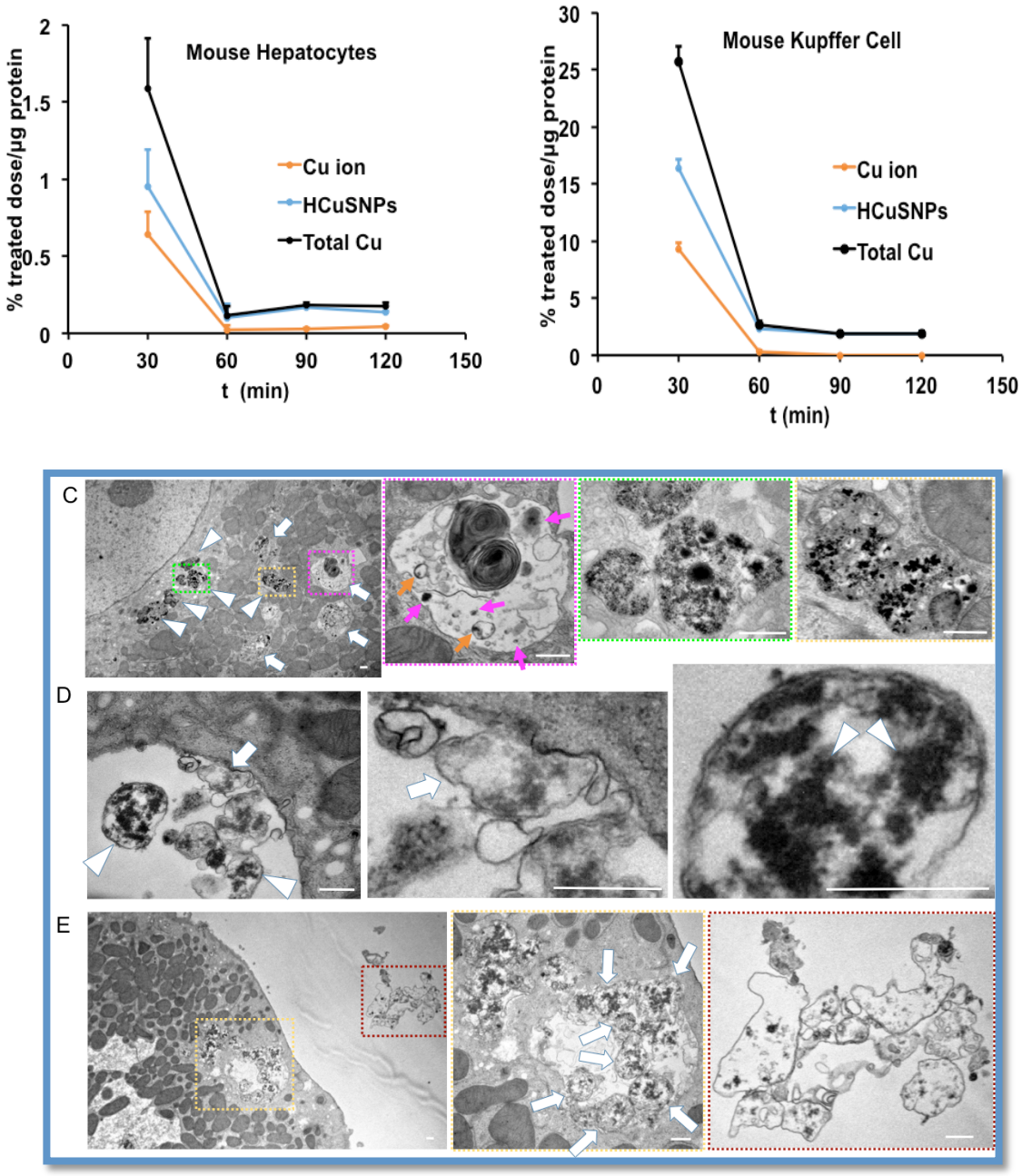

Figure 3. (A), Primarily cultured mouse hepatocytes and Kupffer cells after two steps collagenase perfusion. Mouse primary hepatocytes were seeded in chamber slide pre-coated with collagen. The cells were fixed with cold acetone for 5 min followed by blocking with 10% goat-serum for 30 min at room temperature. The cells were incubated with RbxMs Anti-Cytokeratin 18 Mab (Abcam, 1:100) at 4^{o}C overnight.

After PBS washing for three times, the cells were stained with Alexa Fluor 555 goat anti-rabbit IgG (1:500) for 1 h at room temperature. After PBS washing for 3 times, the cell nuclei were counterstained with DAPI. Mouse primary Kupffer cells were separated through incubation with 10 uL phycoerythrin(PE)-conjugated anti-F4/80 antibody in the dark for 15 min at 4^{o}C, and washed with 1 mL BPE. The cell pellet was then resuspended in 100 uL BPE and incubated with 20 uL anti-PE microbeads (Miltenyi Biotec) in the dark for 15 min at 4 ^{o}C. The cells were seeded on rat tail type I collagen (Corning, Product #354236) coated coverslips. After 24 h, the cells were fixed with cold acetone for 5 min. After PBS washing for three times, the cell nuclei were counterstained with DAPI. Bar, 50 μm. (B), Endocytosis and exocytosis of Cu by primarily cultured mouse hepatocytes and Kupffer cells. Hepatocytes and kupffer cells were incubated with PEG-HCuSNPs (10 μg/mL) pretreated with intact mouse serum for 1 h followed by replacement with fresh media. Cu concentrations in lysate of hepatocytes and Kupffer cells were analyzed. Data are presented as mean ± standard deviation (n = 4). (C-E), TEM of hepatocytes at 1 h following incubation with PEG-HCuSNPs in the presence of 2% intact mouse serum. (C), Distribution of CuS nanoparticles in cells. White arrows, late endosomes; Arrowheads, lysosomes; Pink arrows, decomposed CuS nanoparticles in the late endosome; Orange arrows, decomposed CuS nanoparticles in vacuoles inside the late endosome. (D), Exocytosis of CuS nanoparticles. Arrowheads, nanoparticles in exosomes with decomposed nanostructures; Arrows, an exosome being released directly from the cytoplasm membrane. (E), Multivesicular bodies moving toward cytoplasm membrane and their

exocytosis. Arrow, CuS nanoparticle-loaded vesicles inside the multivesicular bodies. Bars, 500 nm.

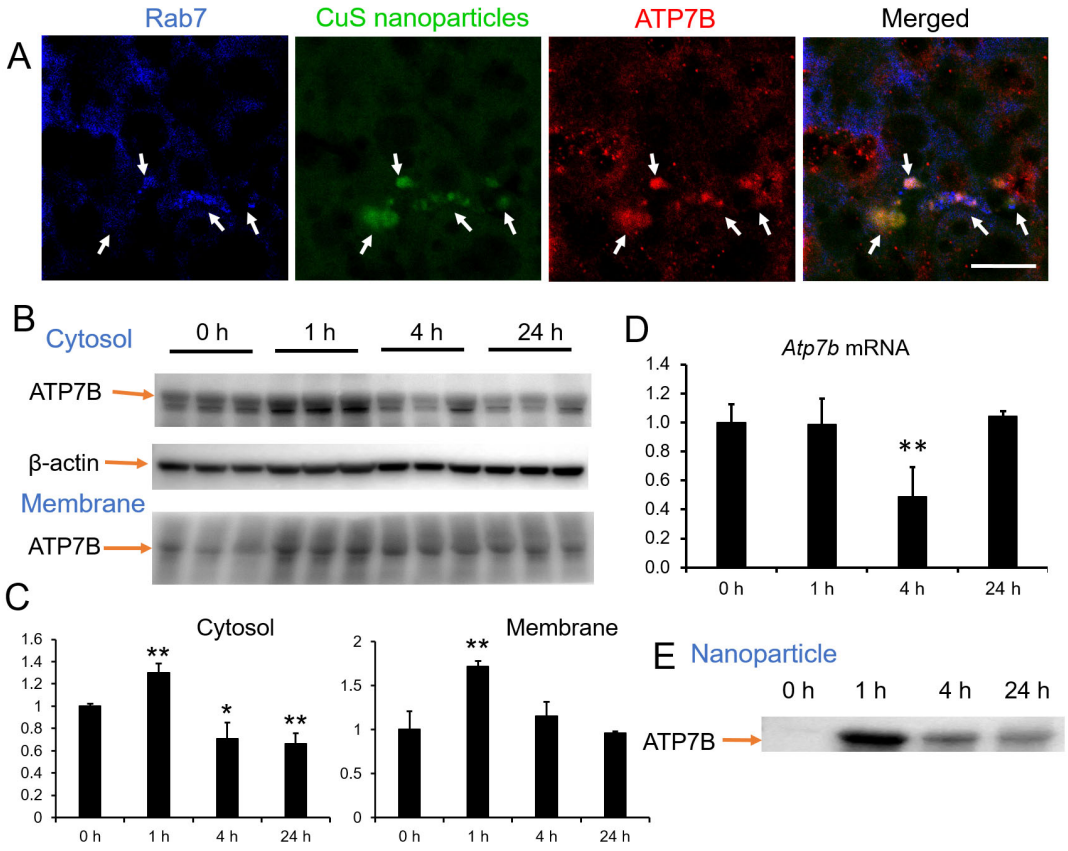

Figure 4. (A), Immunofluorescence imaging of liver in BALB/c mouse at 1 h after receiving i.v. injection of FITC-labeled PEG-HCuSNPs. Blue, late endosomes/lysosomes immunostained with rabbit anti-Rab7 antibody followed by CFL405 conjugated donkey anti-rabbit IgG; Green, FITC-labeled CuS nanoparticles; Red, ATP7B stained with goat anit-ATP7B antibody followed by CFL555 conjugated donkey anti-goat IgG. Arrows, colocalization of three fluorescences. Bar, 10 µm. (B-E), Expression of ATP7B over time in primary hepatocytes isolated from BALB/c mice after i.v. injection of PEG-HCuSNPs (20 mg/kg of Cu). (B), Western-blotting

analysis of ATP7B protein levels over time in cytoplasm (Upper row) or on membrane (Lower row). Three samples collected from three mice at each time point. Control, β-actin (Middle row) in cytosol. "0 h", before injection. (C), Semi-quantitative analysis of ATP7B expression in (B). The gray scale intensity of each sample was normalized with that of β-actin expression. Data are presented as mean ± standard deviation (n=3). **p<0.01, normalized intensity at different times vs. that at 0 h. (D), Quantitative analysis of Atp7b mRNA levels in hepatocytes over time by real-time PCR. Data are presented as mean ± standard deviation (n = 4). **p<0.01, normalized intensity at different times vs. that at 0 h. (E), Western-blot analysis of ATP7B protein adsorbed on CuS nanoparticles in primary hepatocytes from mice following injection. One sample was collected from three mice at each time point.

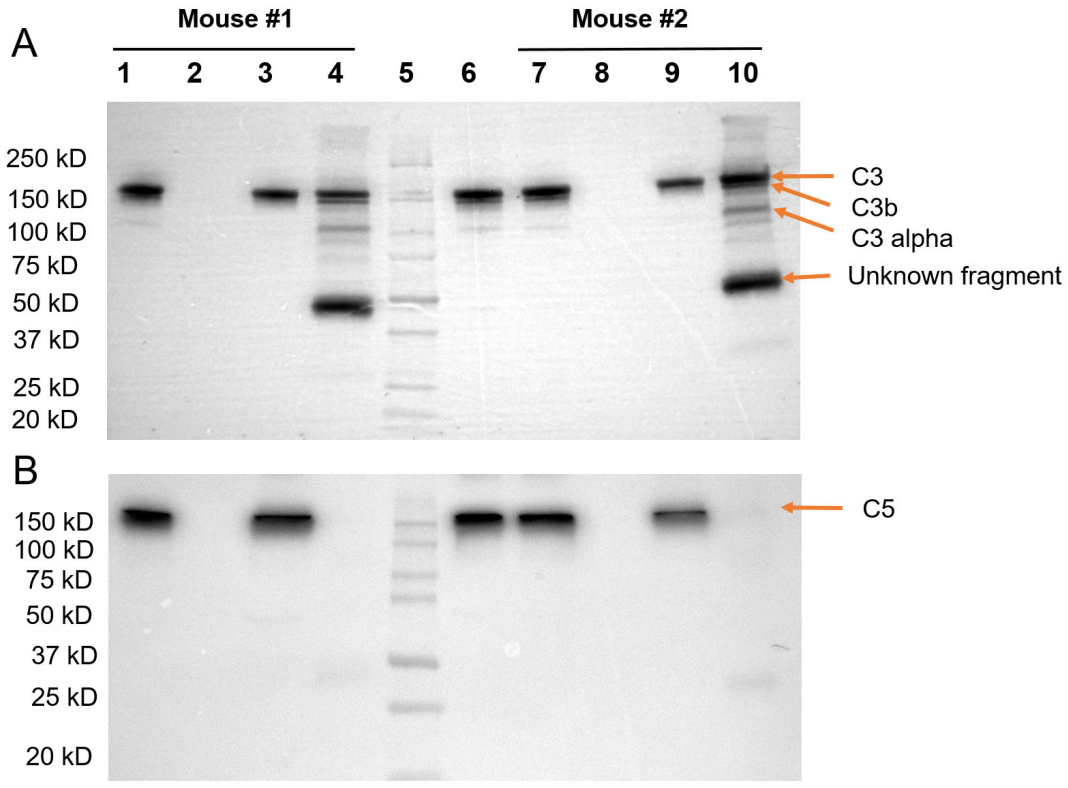

Figure 5. Western blot analysis of complement C3 (A) and C5 (B) on nanoparticle-adsorbed proteins. PEG-HAuNS or PEG-HCuSNPs were incubated for 30 minutes with 10% freshly collected mouse serum from two mice, followed by centrifugation to separate nanoparticles (pellet) from the serum (supernatant). Samples were loaded for Western blotting analysis using rat anti-mouse C3 mAb or rat anti-mouse C5a mAb as first antibody. Lanes (1) and (7), supernatant from PEG-HAuNS-incubated serum; Lanes (2) and (8), PEG-HAuNS-bound protein (pellet); Lanes (3) and (9), supernatant from PEG-HCuSNPs-incubated serum; Lanes (4) and (10), PEG-HCuSNPs-bound protein (pellet); Lane (6), diluted freshly collected mouse serum; Lane (5), protein ladders.

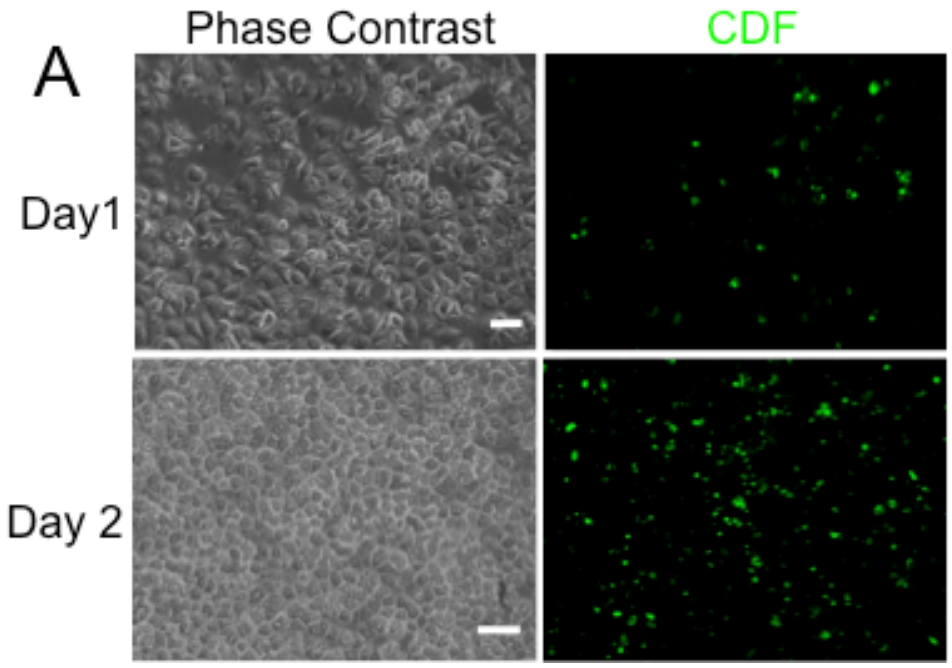

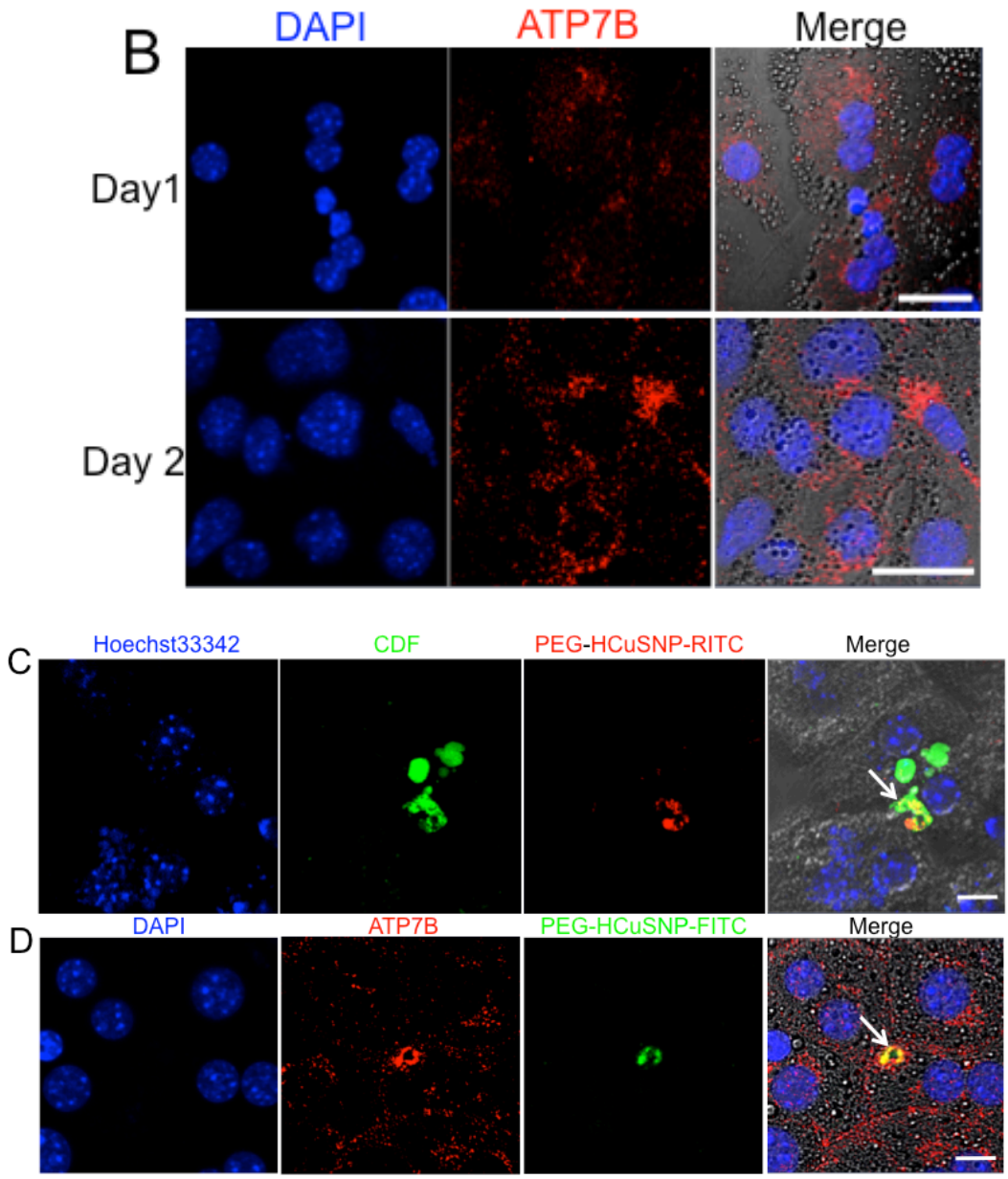

Figure 6. The primarily isolated mouse hepatocyte could form the bile canaliculus and functional to excrete the HCuSNPs after two days incubation (A), Confocal image of bile canaliculus after 2 days primarily isolated mouse hepatocyte incubation. Mouse primary hepatocytes were seeded in 35mm petri-dish pre-coated with rat tail type I collagen and incubated for 48 hours. Cells were washed twice with 1ml pre-warmed HBSS (with Ca^{2+}/Mg^{2+}). Then, 1 ml of pre-warmed HBSS (with Ca^{2+}/Mg^{2+})

containing 5μM CDFDA was added and incubated cells for 20 minutes in a 37°C incubator with 5% CO_2. At the end of the incubation, aspirated medium and washed cells twice with 1 ml pre-warmed HBSS (with Ca^{2+}/Mg^{2+}) buffer. Assess cell morphology and bile canaliculi formation (CDF accumulation in bile canaliculi) with Zeiss LSM 700 confocal microscope. Bar 100μm. (B), Immunofluorescence imaging of ATP7B in mouse hepatocytes after two days incubation. Red, ATP7B stained with goat anit-ATP7B antibody followed by Alexa Fluor 555-conjugated donkey anti-goat IgG. Blue, DAPI. Bar, 10 μm. (C), Immunofluorescence imaging of HCuSNPs excretion into bile canaliculus. Green, CDF; Red, PEG-HCuSNP-RITC; Blue, Hoechst33342-labeled cell nuclei. Arrows, colocalization of two fluorescences. Bar, 10 μm. (D), Immunofluorescence imaging of HCuSNPs colocalized with ATP7B. Red, ATP7B; Green, PEG-HCuSNP-FITC; Blue, DAPI-labeled cell nuclei. Bar, 10 μm.

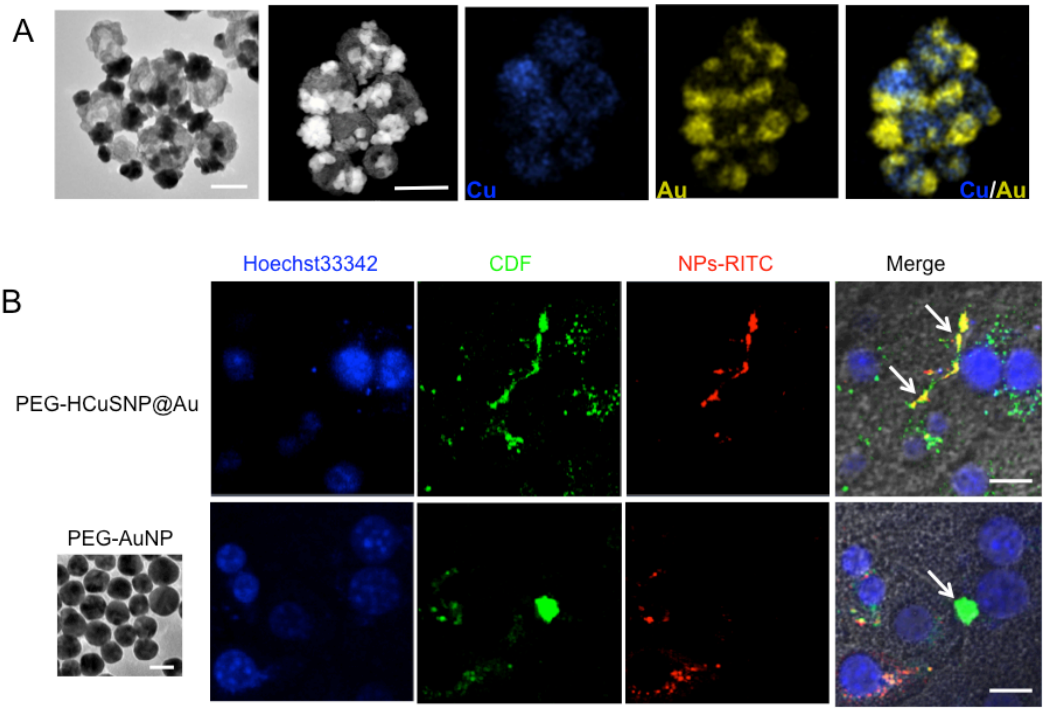

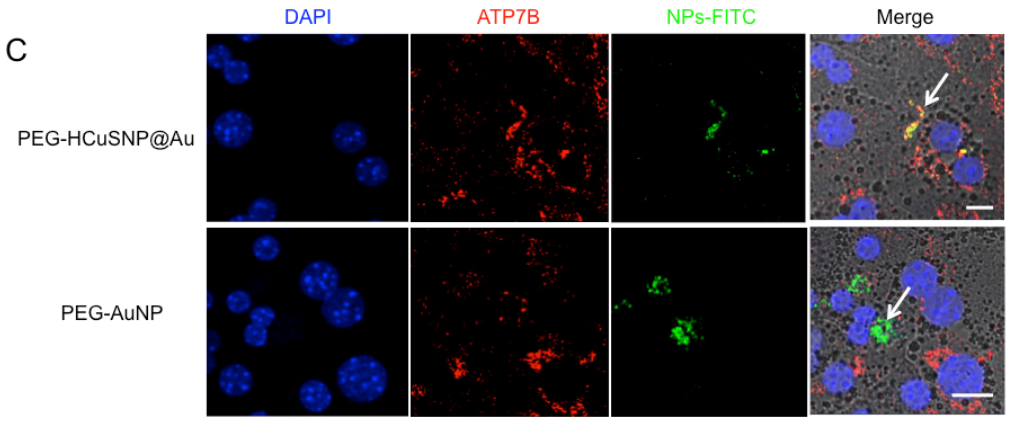

Figure 7. (A), TEM of PEG-HCuSNP@Au. Bar 100nm. (B), Immunofluorescence imaging of PEG-HCuSNP@Au and PEG-AuNP excretion. Green, CDF; Red, PEG-NP-RITC; Blue, Hoechst33342-labeled cell nuclei. Arrows, colocalization of two fluorescences. (C), Immunofluorescence imaging of PEG-HCuSNP@Au and PEG-AuNP localization relative to ATP7B. Red, ATP7B; Green, PEG-NP-FITC; Blue, DAPI-labeled cell nuclei. Bar, 10 µm. TEM bar for PEG-AuNP is 50nm.

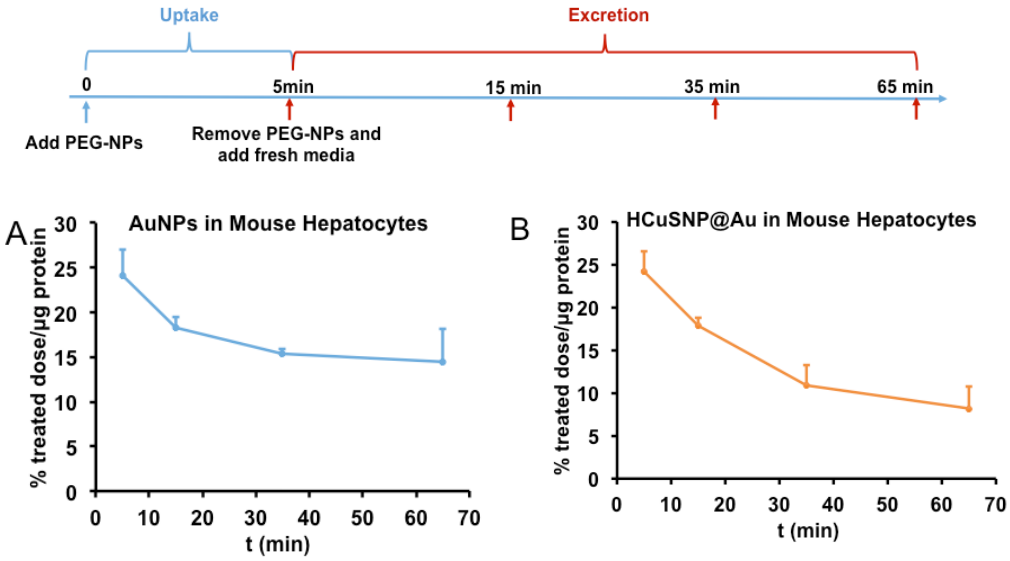

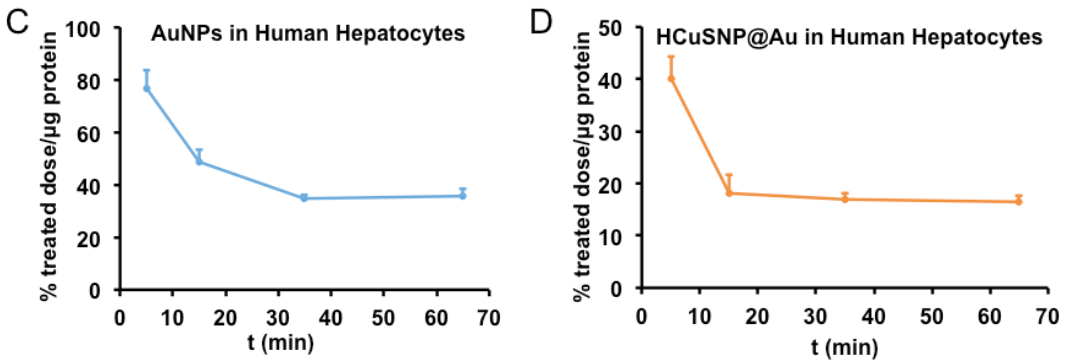

Figure 8. (A)(B), Comparison of cellular endocytosis and exocytosis between AuNP and HCuSNP@Au conjugation by mouse primary hepatocytes. 300,000 mouse primary hepatocytes were seeded on collagen coated 12 mm-insert Transwell (Corning) for 48h. Before treating the cells, AuNP and HCuSNPs@Au were incubated in the mouse serum for 1 hour. The final mouse serum concentration in DMEM was 2%. Then mouse serum containing AuNP or HCuSNPs@Au were added to each transwell to treat the cells for 5 min to test the cellular endocytosis of nanoparticles. In a separated set of transwells, after treating the cells for 5 min, transwells were washed and the media was replaced with fresh DMEM plus 10% FBS and incubated with the cells for another 10, 30, 60 min to determine the cellular exocytosis of AuNP or HCuSNPs@Au. The mouse serum used in this study was freshly collected from BALB/C mouse blood in the same day of this experiment. (C)(D), Comparison of cellular endocytosis and exocytosis between AuNP and HCuSNP@Au by human primary hepatocytes.

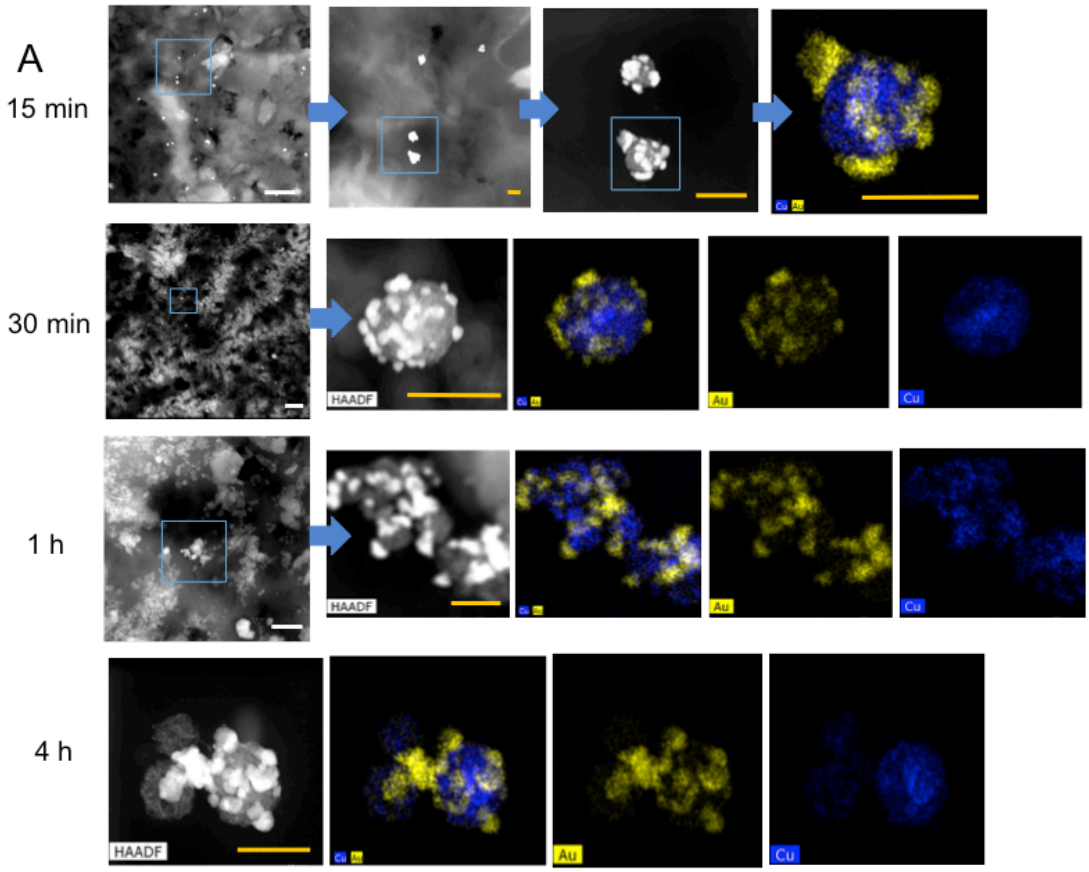

Figure 9. TEM of bile samples collected from BALB/c mice at 15min, 30min, 1h and 4h following i.v. injection of PEG-HCuSNP@Au. Bars in white, 1μm; Bars in yellow, 100 nm.

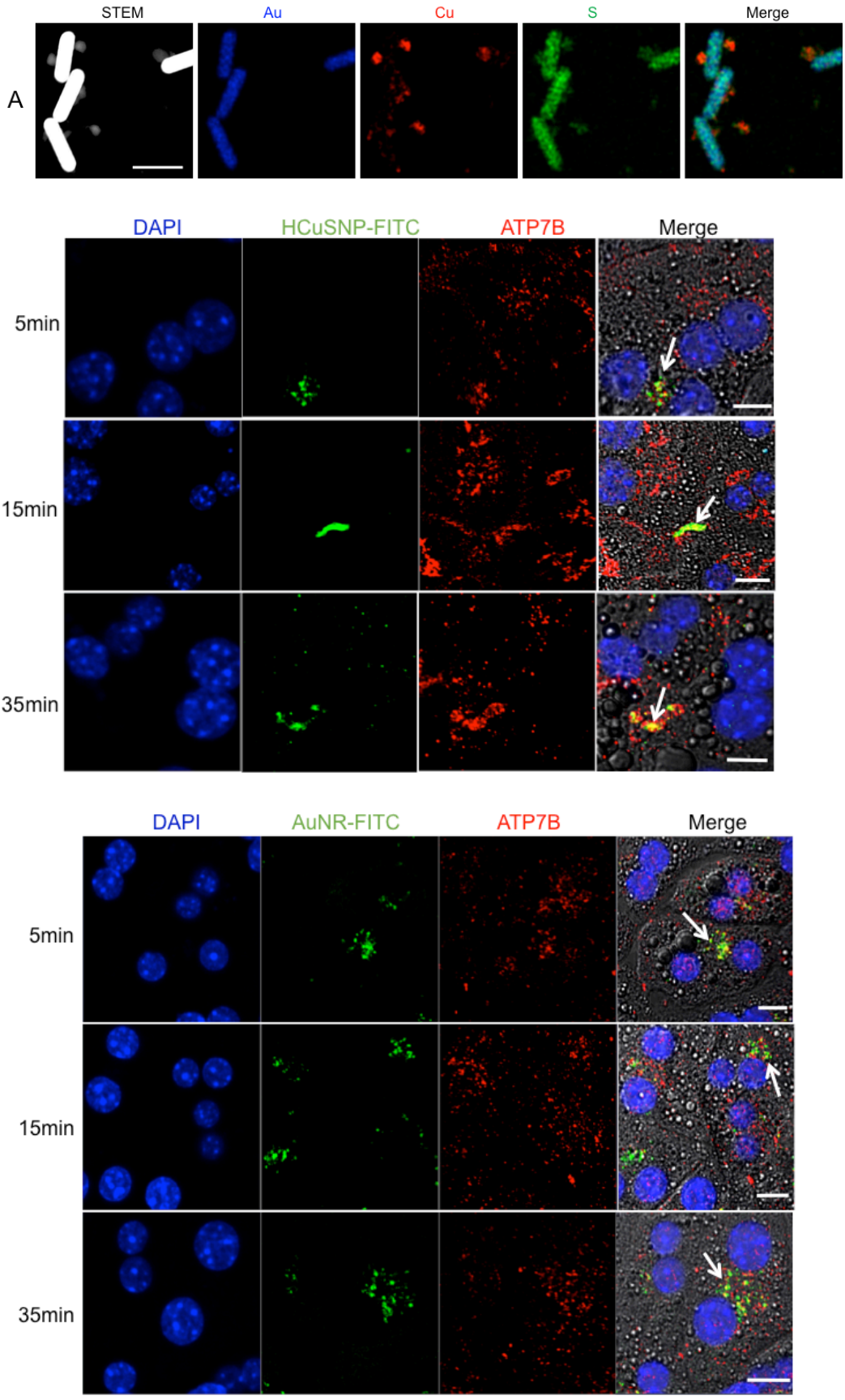
A
STEM
Au
Cu
S
Merge
B
DAPI
HCuSNP-FITC
ATP7B
Merge
5min
15min
35min
C
DAPI
AuNR-FITC
ATP7B
Merge
5min
15min
35min

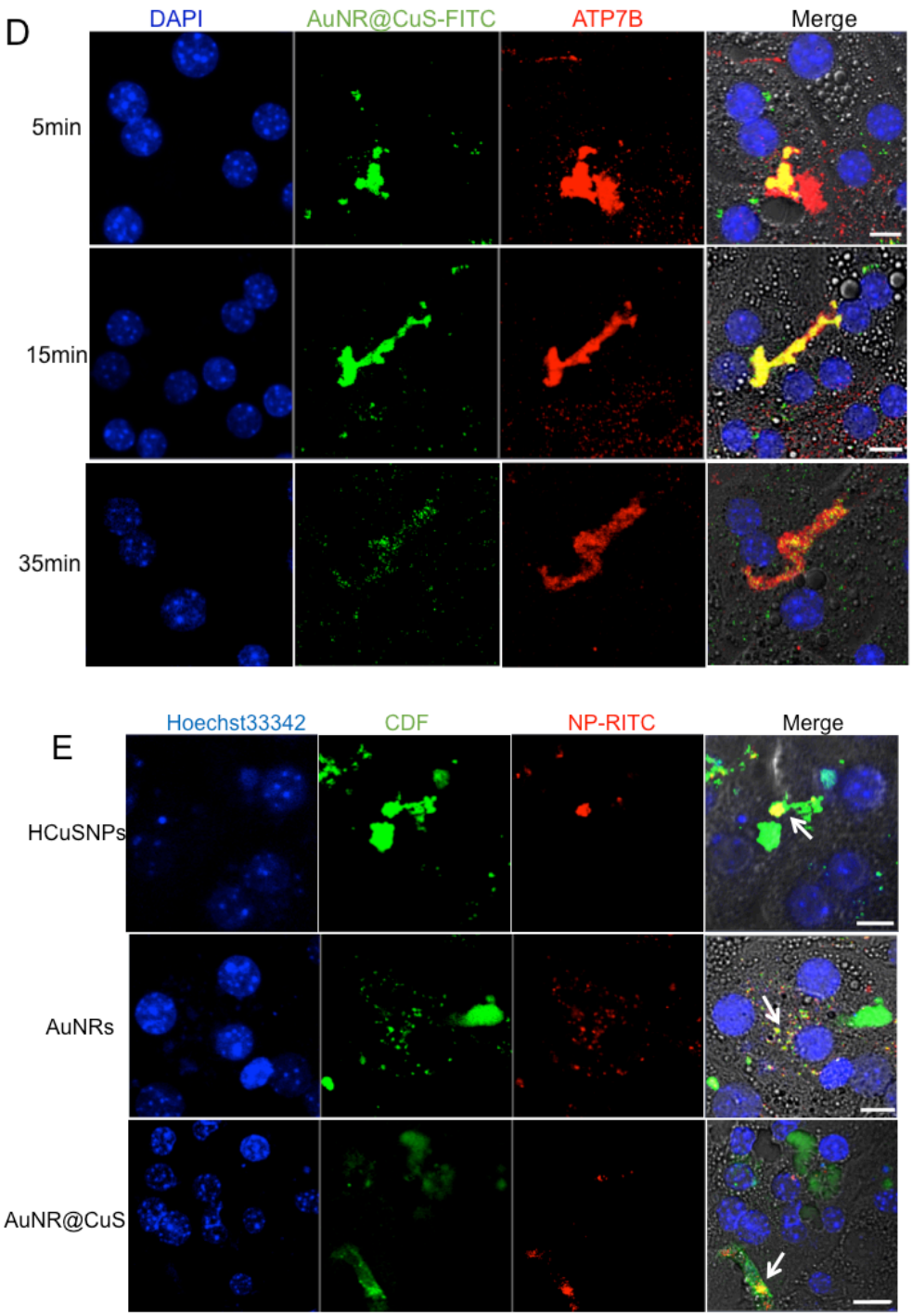

Figure 10. (A) TEM of AuNR@CuS. Bar 40nm. (B-D) Immunofluorescence imaging of NPs location relative to ATP7B at 5min, 15min and 35min treatment. Red, ATP7B; Green, PEG-NP-FITC; Blue, DAPI-labeled cell nuclei. (B),HCuSNPs (C), AuNR (D), AuNR@CuS. (E) Immunofluorescence imaging of NPs excretion into bile

canaliculus after 35 min incubation. Green, CDF; Red, PEG-NP-RITC; Blue, Hoechst33342-labeled cell nuclei. Bar is 10μm in (B-E). Arrows, colocalization of two fluorescences.

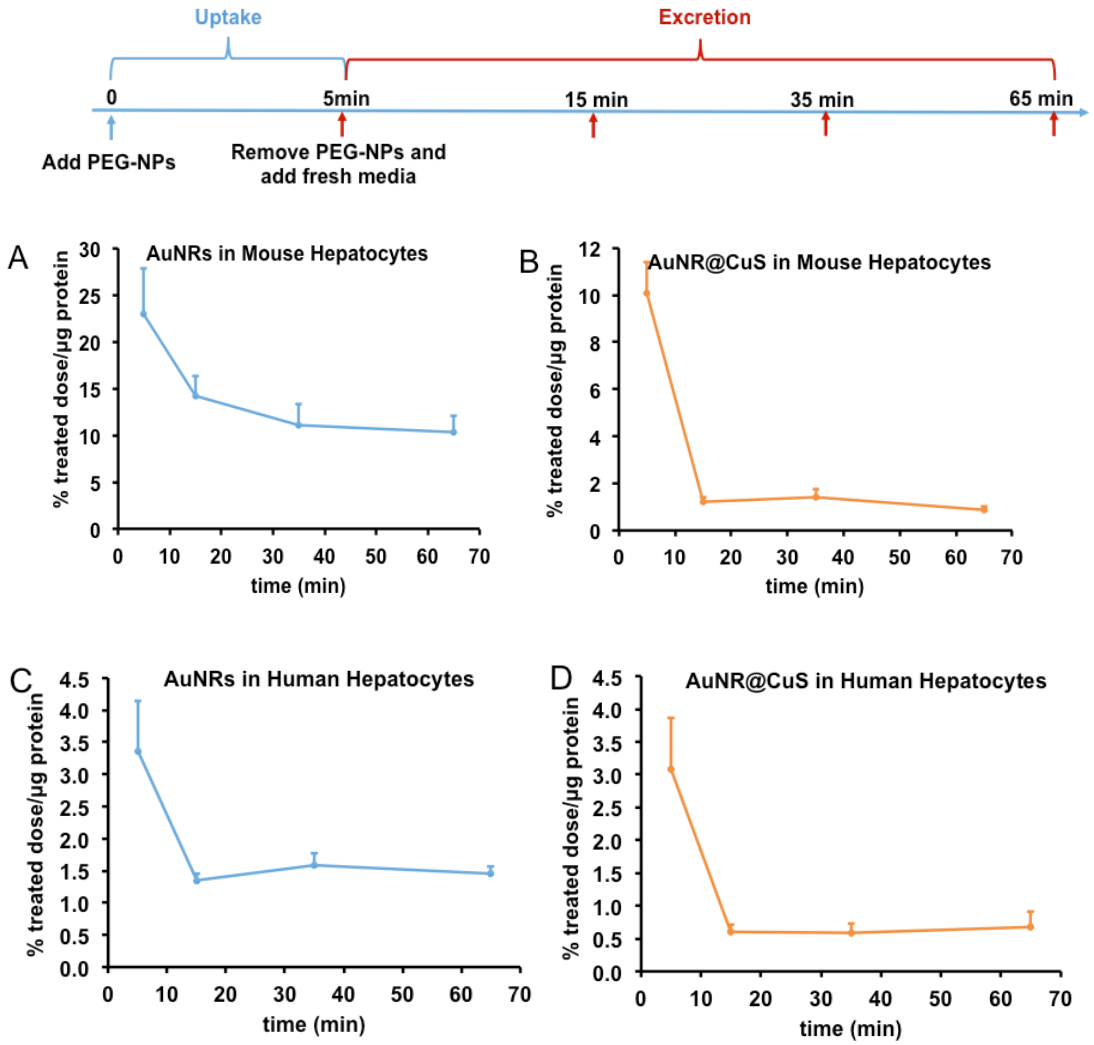

Figure 11. (A)(B), Comparison of cellular endocytosis and exocytosis between AuNR and AuNR@CuS conjugation by mouse primary hepatocytes. 300,000 mouse primary hepatocytes were seeded on collagen coated 12 mm-insert Transwell (Corning) for 48h. Before treating the cells, AuNR and AuNR@CuS were incubated in the mouse

serum for 1 hour. The final mouse serum concentration in DMEM was 2%. Then mouse serum containing AuNR and AuNR@CuS were added to each transwell to treat the cells for 5 min to test the cellular endocytosis of nanoparticles. In a separated set of transwells, after treating the cells for 5 min, transwells were washed and the media was replaced with fresh DMEM plus 10% FBS and incubated with the cells for another 10, 30, 60 min to determine the cellular exocytosis of AuNR and AuNR@CuS. The mouse serum used in this study was freshly collected from BALB/C mouse blood in the same day of this experiment. (C)(D), Comparison of cellular endocytosis and exocytosis between AuNR and AuNR@CuS conjugation by human primary hepatocytes.

Table 1. Comparison of the number of proteins absorbed to PEG-HCuSNPs at 5 min and at 1 h after i.v. injection.*

Biological process	N (Number of proteins)		$N_{1\ h}/N_{5\ min}$
	5 min	1 h	
Biological adhesion	5	51	10.2
Biological regulation	13	271	20.8
Cell killing	1	7	7.0
Cellular process	14	383	27.4
Developmental process	7	171	24.4
Establishment of localization	6	128	21.3
Growth	1	13	13.0
Immune system process	5	73	14.6

Viral reproduction	0	4	-
Unknown	23	82	3.6
Rhythmic process	1	7	7.0
Response to stimulus	9	176	19.6
Reproductive process	1	18	18.0
Reproduction	1	20	20.0
Pigmentation	0	1	-
Multicellular organismal process	10	167	16.7
Multi-organism process	1	29	29.0
Metabolic process	6	251	41.8
Locomotion	2	40	20.0
Localization	7	155	22.1

*Protein classification was based on the biological process in gene ontology terms.

Table 2. A representative characterization of the 10 most abundant proteins adsorbed to PEG-HCuSNPs separated from mouse plasma at 5 min after i.v. injection.

	Protein	%Spec
1	Complement C3	0.067
2	Ig mu chain C region (Fragment)	0.053
3	Kininogen-1	0.047
4	Potassium voltage-gated channel subfamily KQT member 5	0.020
5	Isoform Kidney of Band 3 anion transport protein	0.020
6	Keratin, type II cytoskeletal 2 oral	0.013
7	Hemoglobin subunit beta-1	0.013
8	Desmoglein-1-alpha	0.013
9	Ankyrin-1	0.013
10	Isoform 2 of Gelsolin	0.013

Table 3. A representative characterization of the 10 most abundant proteins adsorbed to PEG-HCuSNPs separated from mouse plasma at 1 h after i.v. injection.

	Protein	%Spec
1	Complement C3	1.026
2	Myosin-9	0.894
3	Filamin-A	0.635
4	Hemoglobin subunit alpha	0.485
5	Talin-1	0.409

6	Hemoglobin subunit beta-1	0.348
7	Actin, cytoplasmic 1	0.309
8	Beta-globin	0.305
9	Serum albumin	0.248
10	ATP synthase subunit beta, mitochondrial	0.240

Graphical Table of Contents

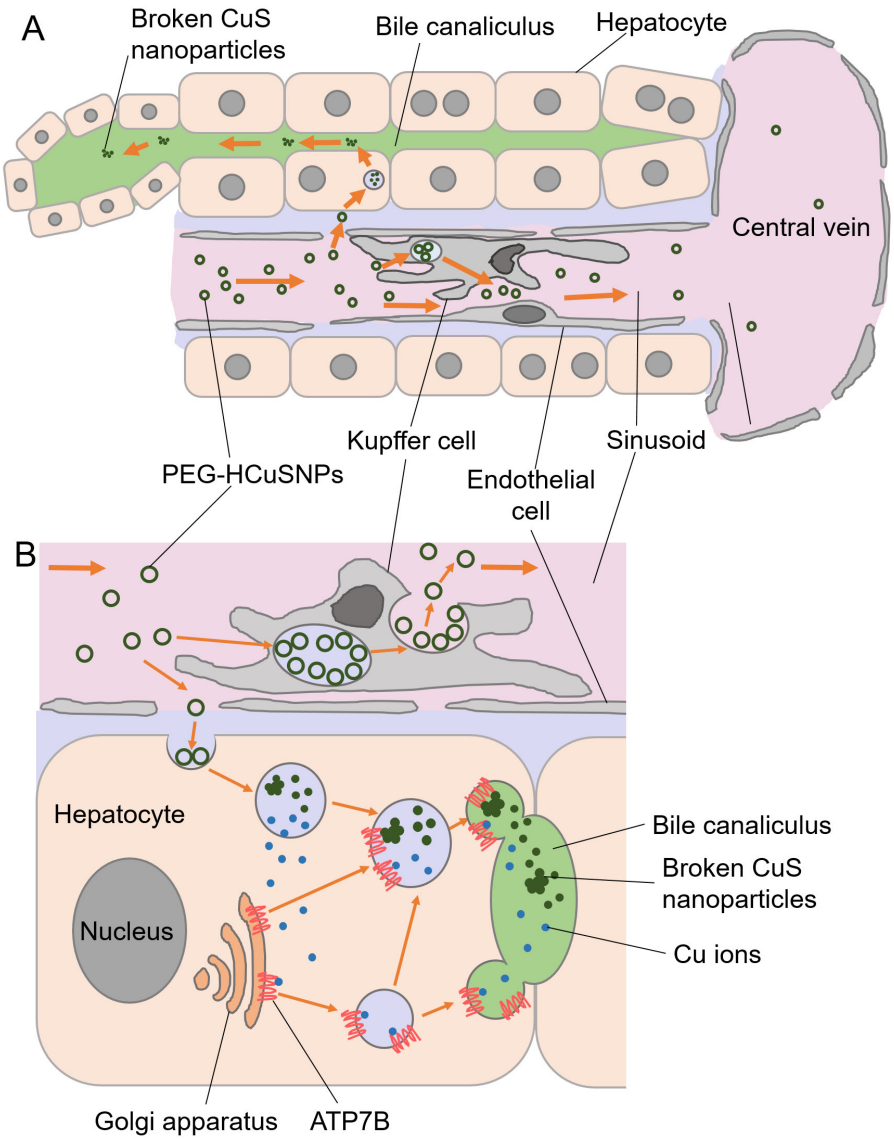

Scheme 1. (A), Illustration showing two distinct pathways of PEG-HCuSNPs in hepatocytes and Kupffer cells following i.v. injection. (B), Detailed metabolic process of PEG-HCuSNPs in (A).

Supporting Information

Enhanced Cellular Clearance of Gold Nanoparticles by Copper Sulfide Nanoparticles Through ATP7B as Transporter

Xiaodong Wang,[‡] Liangran Guo,[‡,] Yi-Tzai Chen,[‡,] Yuan Chen,[‡,] Yixin Chen,[‡] Bingfang Yan,[‡] Wei Lu[†,‡,*]

[†]Department of Pharmaceutics, School of Pharmacy, Key Laboratory of Smart Drug Delivery, Ministry of Education, & State Key Laboratory of Molecular Engineering of Polymers, Fudan University, Shanghai 201203, China; [‡]Department of Biomedical and Pharmaceutical Sciences, College of Pharmacy, The University of Rhode Island, Kingston, Rhode Island 02881, United States.

*Corresponding author: Department of Pharmaceutics, School of Pharmacy, Key Laboratory of Smart Drug Delivery, Ministry of Education, & State Key Laboratory of Molecular Engineering of Polymers, Fudan University, 826 Zhangheng Road, Shanghai 201203, China. Phone: +86-21-51980185. Fax: +86-21-51980184. E-mail: wlu@fudan.edu.cn

EXPERIMENTAL SECTION

Dissolution study of PEG-HCuSNPs. PEG-HCuSNPs (0.1 mg/mL of Cu) were dispersed and incubated in 10 mL of various media in glass vials stirring at 200 rpm. At predetermined time points, 0.5 mL of samples were transferred to Eppendorf tubes and centrifuged at 21,130 *g*. The supernatant were carefully collected for inductively coupled plasma mass spectrometer (ICP-MS) analysis (Model: X7, Thermo Electron Corporation) of Cu. The samples were also examined under TEM (JEOL, JEM2100).

Labeling PEG-HCuSNPs with fluorescein isothiocyanate (PEG-HCuSNPs-FITC) and FITC release. FITC-maleimide solution was added to the PEG-HCuSNPs suspension to make a final concentration of 1 mg/mL copper and 0.05 mg/mL of FITC-maleimide. After stirring for 48 h, the obtained PEG-HCuSNPs-FITC were washed with deionized water 5 times and further with dimethylsulfoxide (DMSO) twice to remove the unconjugated FITC-maleimide. To test FITC released from PEG-HCuSNPs-FITC, PEG-HCuSNPs-FITC were suspended in 10 mL of acetic buffer (pH 4.9) or PBS (7.4) containing 10% mouse serum, and stirred at 200 rpm. At predetermined time points, 0.5 mL of samples were collected followed by centrifugation. The fluorescence of FITC in the supernatant was quantified by microplate reader (Spectramax M2, Ex= 485 nm; Em = 538 nm; cut-off = 530 nm).

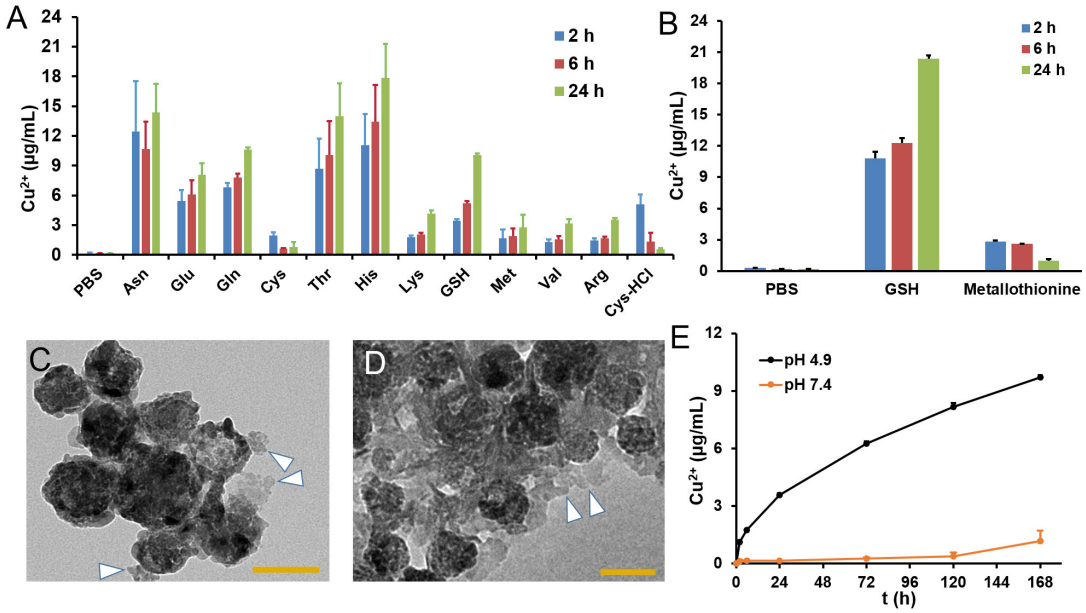

Figure S1. Dissociation of PEG-HCuSNPs (0.1 mg/mL of Cu) in various media at different time points. (A), The concentration of Cu^{2+} released from PEG-HCuSNPs in PBS alone, or PBS supplemented with various amino acids (2 mM). (B), The concentration of Cu^{2+} released from PEG-HCuSNPs in PBS alone, or PBS supplemented with GSH (2 mM) or metallothionine (30 μg/mL). (C-D), TEMs of PEG-HCuSNPs in PBS containing 2 mM of GSH (C) or in PBS containing 30 μg/mL of metallothionein (D) after 24-h incubation. Arrowheads, dissociated CuS particles. Bars, 100 nm. (E), Cu^{2+} dissolution from PEG-HCuSNPs in acetic buffer (pH 4.9) or PBS (pH 7.4). Data are presented as mean ± standard deviation (n = 3).

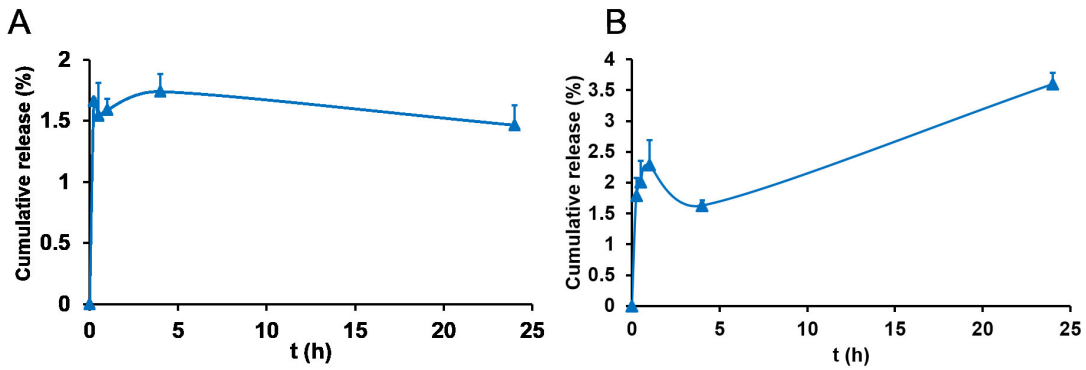

Figure S2. Cumulative release of FITC from the FITC-conjugated PEG-HCuSNPs (PEG-HCuSNPs-FITC) in acetate buffer (pH 4.9) (A), or PBS containing 10% mouse serum (B). Data are presented as mean ± standard deviation (n = 3).

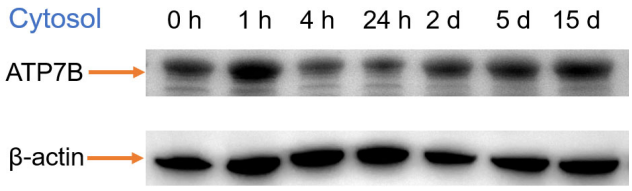

Figure S3. Western-blot analysis of ATP7B protein levels in cytoplasm of hepatocytes in mice over 15 d after i.v. injection of PEG-HCuSNPs.